




## Article

# Singularity-Free and Cosmologically Viable Born-Infeld Gravity with Scalar Matter

David Benisty <sup>1,2</sup> , Gonzalo J. Olmo <sup>3</sup>  and Diego Rubiera-Garcia <sup>4,\*</sup> 
<sup>1</sup> DAMTP, Centre for Mathematical Sciences, University of Cambridge, Wilberforce Road, Cambridge CB3 0WA, UK; benidav@post.bgu.ac.il

<sup>2</sup> Kavli Institute of Cosmology (KICC), University of Cambridge, Madingley Road, Cambridge CB3 0HA, UK

<sup>3</sup> Departamento de Física Teórica and IFIC, Centro Mixto Universidad de Valencia—CSIC, Universidad de Valencia, Burjassot, E-46100 Valencia, Spain; gonzalo.olmo@uv.es

<sup>4</sup> Departamento de Física Teórica and IPARCOS, Universidad Complutense de Madrid, E-28040 Madrid, Spain

\* Correspondence: drubiera@ucm.es

**Abstract:** The early cosmology, driven by a single scalar field, both massless and massive, in the context of Eddington-inspired Born-Infeld gravity, is explored. We show the existence of nonsingular solutions of bouncing and loitering type (depending on the sign of the gravitational theory's parameter,  $\epsilon$ ) replacing the Big Bang singularity, and discuss their properties. In addition, in the massive case, we find some new features of the cosmological evolution depending on the value of the mass parameter, including asymmetries in the expansion/contraction phases, or a continuous transition between a contracting phase to an expanding one via an intermediate loitering phase. We also provide a combined analysis of cosmic chronometers, standard candles, BAO, and CMB data to constrain the model, finding that for roughly  $|\epsilon| \lesssim 5 \cdot 10^{-8} \text{ m}^2$  the model is compatible with the latest observations while successfully removing the Big Bang singularity. This bound is several orders of magnitude stronger than the most stringent constraints currently available in the literature.

**Keywords:** metric-affine gravity; non-singular cosmologies; born-infeld gravity; observational constraints; scalar fields



**Citation:** Benisty, D.; Olmo, G.J.; Rubiera-Garcia, D. Singularity-Free and Cosmologically Viable Born-Infeld Gravity with Scalar Matter. *Symmetry* **2021**, *13*, 2108. <https://doi.org/10.3390/sym13112108>

Academic Editor: Kazuharu Bamba

Received: 21 April 2021

Accepted: 29 October 2021

Published: 6 November 2021

**Publisher's Note:** MDPI stays neutral with regard to jurisdictional claims in published maps and institutional affiliations.



**Copyright:** © 2021 by the authors. Licensee MDPI, Basel, Switzerland. This article is an open access article distributed under the terms and conditions of the Creative Commons Attribution (CC BY) license (<https://creativecommons.org/licenses/by/4.0/>).

## 1. Introduction

The standard concordance cosmological  $\Lambda$ CDM model, framed within Einstein's General Theory of Relativity (GR), including an early phase of inflationary expansion, a cold dark-matter component, and a tiny cosmological constant driving the accelerated late-time expansion of the Universe, has successfully met all observations [1,2]. Within this model, scalar fields have found new and imaginative applications. For instance, inflationary models in the early Universe involve from one to many scalar fields [3–12]. In the slow-roll approximation the exact form of the scalar field potential is unknown, since many different potentials have been studied and confronted to observations. On the other hand, a way to parameterize dark energy is by using a scalar field, the so-called quintessence model (for canonical scalar fields [13,14]) or its generalizations to K-essence models (when a non-canonical scalar Lagrangian is considered [15–18]), in such a way that the cosmological constant is replaced by a dark energy fluid with a nearly constant density [19–23]. Dark matter can be also parameterized in terms of weakly interacting massive particles, which can be scalar particles that are still undiscovered at colliders and other dark matter detection experiments. Models for dark matter can also be based on other kinds of scalar fields, for instance, via fuzzy dark matter [24], or by using a Lagrange multiplier that changes the behaviour of the kinetic term [25–28]. Scalar field models may also be the result of complex effective interactions between other fundamental fields in equilibrium, such as in Bose–Einstein condensates, thus allowing for an even broader range of phenomenological justifications. Therefore, the consideration of scalar fields within cosmological models

is justified when building a fully consistent history of the cosmological evolution that is compatible with observations.

On the gravity side, and despite its observational success, from a fundamental perspective the  $\Lambda$ CDM model still contains a visible singularity at the Universe's past. This is an unavoidable consequence of the singularity theorems (see, e.g., [29] for a pedagogical discussion). To tackle this issue, it is widely assumed in the community that at the strong curvatures and fields of the very early Universe, quantum gravity effects should come into play to regularize this singularity. Since a quantum theory of gravity is not available to date, an effective way to capture such hypothetical effects is via modified theories of gravity [30–33]. The plausibility of such alternative gravitational descriptions to supersede GR and represent observationally viable alternatives to the  $\Lambda$ CDM model has been widely discussed in the literature, according to different perspectives and approaches [34].

Among the large pool of theories which have been investigated in the literature, for the sake of this paper, we present the proposal that was originally introduced by Banados and Ferreira [35] and dubbed Eddington-inspired Born-Infeld (EiBI) gravity (This proposal can actually be framed within the tradition of considering square-root action, such as in the DBI one, e.g., [36–39]). To avoid troubles with ghost-like instabilities, this theory is typically formulated in metric-affine spaces, where metric and affine connection are *a priori* independent entities. EiBI theory has found many different applications in astrophysics and cosmology, e.g., [40–49]. In particular, the existence of bouncing solutions replacing the Big Bang singularity within EiBI gravity was first hinted at in [50], when scalar fields are considered as the matter source. Further works on the subject in recent years have reinforced the ability of this theory to remove such singularities according to different mechanisms (for a review, see [51]).

The main aim of this work is to construct explicit such singularity-free solutions within the early cosmological evolution, corresponding to a single, massless (quintaessential) scalar field, and to further (numerically) extend this analysis to the massive case. We shall show the existence of two kinds of singularity-free solutions depending on the sign of the EiBI gravity parameter. The first one corresponds to bouncing solutions, where the universe contracts down to a minimum size before entering into an expansion phase, while the second are loitering solutions, which interpolate between an asymptotically Minkowski past and the current cosmological evolution. For these nonsingular solutions, we carry out a combined analysis of cosmic chronometers, standard candles, BAO, and CMB data in order to constrain the EiBI parameter, finding the bound  $|\epsilon| \lesssim 5 \cdot 10^{-8} \text{ m}^2$ .

This paper is organized as follows: in Section 2 we introduce EiBI gravity, discuss its properties, and construct its cosmological equations when coupled to a scalar field. In Section 3 we consider massless scalar fields and discuss their corresponding bouncing and loitering solutions, extending these results in Section 4 to the massive case. Section 5 sees the theory fit with the latest observations (on  $\Lambda$ CDM background), and we conclude in Section 6 with a summary and some perspectives.

## 2. Eddington-Inspired Born-Infeld Gravity

### 2.1. Action and Basic Field Equations

The action of EiBI gravity can be conveniently written as

$$\mathcal{S}_{\text{EiBI}} = \frac{1}{\epsilon \kappa^2} \int d^4x [\sqrt{-q} - \lambda \sqrt{-g}] + \mathcal{S}_m(g_{\mu\nu}, \psi_m), \quad (1)$$

where  $\kappa^2 \equiv 8\pi G/c^4$  is Newton's constant,  $\epsilon$  is EiBI parameter,  $\lambda$  is a dimensionless constant,  $g$  is the determinant of the space-time metric  $g_{\mu\nu}$  and  $q$  the determinant of an auxiliary metric defined as:

$$q_{\mu\nu} \equiv g_{\mu\nu} + \epsilon R_{(\mu\nu)}(\Gamma), \quad (2)$$

where the (symmetric part of the) Ricci tensor  $R_{\mu\nu}(\Gamma) \equiv R^\rho{}_{\mu\rho\nu}(\Gamma)$  is a function solely of the (torsionless) affine connection  $\Gamma \equiv \Gamma^\lambda_{\mu\nu}$ , assumed to be *a priori* independent of the

space–time metric  $g_{\mu\nu}$  (metric-affine or Palatini formalism). This symmetrizing requirement ensures that the theory is invariant under projective transformations, which avoids the presence of ghost-like instabilities [52,53]. For the matter sector,  $\mathcal{S}_m = \int d^4x \sqrt{-g} \mathcal{L}_m(g_{\mu\nu}, \psi_m)$ , it is assumed to be minimally coupled to the space–time metric  $g_{\mu\nu}$  (e.g., [54] for a definition of minimal coupling in metric-affine theories), with  $\psi_m$  collectively denoting the matter fields. It is worth pointing out that EiBI gravity recovers the GR dynamics and its solutions in the  $|R_{\mu\nu}| \ll \epsilon^{-1}$  limit [51] (from now on, vertical bars indicate a determinant), inheriting an effective cosmological constant  $\Lambda_{eff} = \frac{\lambda-1}{\epsilon\kappa^2}$ . This fact allows EiBI gravity to naturally pass weak-field limit tests, such as those based on solar system observations.

EiBI gravity is a very well known theory in the community thanks to its many applications (for a detailed account of its properties, we refer the reader to the review [51]). It is actually a member of the so-called Ricci-based family of gravitational theories [55], all of which admit an Einstein-like representation of their field equations given by

$$G^\mu{}_\nu(q) = \frac{\kappa^2}{|\Omega|^{1/2}} \left[ T^\mu{}_\nu - \delta^\mu_\nu \left( \mathcal{L}_G + \frac{T}{2} \right) \right], \quad (3)$$

where  $\mathcal{L}_G$  is the gravitational Lagrangian,  $T_{\mu\nu} = \frac{2}{\sqrt{-g}} \frac{\delta \mathcal{S}_m}{\delta g^{\mu\nu}}$  is the stress-energy tensor of the matter fields,  $T$  its trace, and  $G^\mu{}_\nu(q)$  is the Einstein tensor of the auxiliary metric  $q_{\mu\nu}$ , such that  $\Gamma$  is the Levi–Civita, that is

$$\nabla_\alpha (\sqrt{-q} q^{\mu\nu}) = 0. \quad (4)$$

This  $q_{\mu\nu}$  metric is related to the space–time one  $g_{\mu\nu}$  via the relation

$$q_{\mu\nu} = g_{\mu\alpha} \Omega^\alpha{}_\nu, \quad (5)$$

where the *deformation* matrix  $\hat{\Omega}$  depends on-shell on the matter fields (and possibly the space–time metric  $g_{\mu\nu}$  as well). For EiBI gravity, this matrix is implicitly determined via the equation

$$|\Omega|^{1/2} (\Omega^{-1})^\mu{}_\nu = \lambda \delta^\mu_\nu - \epsilon \kappa^2 T^\mu{}_\nu, \quad (6)$$

while the EiBI Lagrangian in (1) can also be expressed in terms of this matrix as

$$\mathcal{L}_G = \frac{|\Omega|^{1/2} - \lambda}{\epsilon \kappa^2}. \quad (7)$$

Let us point out that all terms on the right-hand side of the Equations (3) are functions of the matter fields and the metric  $g_{\mu\nu}$ , thus representing a system of second-order field equations with new couplings engendered by the matter fields. In a vacuum,  $T^\mu{}_\nu = 0$ , one recovers the GR solutions (As a remark, we would like to note that it has been shown that in generic RBGs, due to the non-linearities of the field equations, the deformation matrix admits other (typically pathological) solutions besides the one that boils down to GR in vacuum. These solutions can lead to anisotropic deformation matrices even if the stress–energy tensor is isotropic. Remarkably, it was shown that for EiBI gravity, that no such anisotropic solutions exist in the presence of an isotropic stress-energy tensor, see [56].), which ensures the propagation of the two polarizations of the gravitational field travelling at the speed of light [57].

## 2.2. EiBI Cosmology with Scalar Fields

As the matter sector of our model let us consider a single (real) scalar field described by the action

$$\mathcal{S}_m = -\frac{1}{2} \int d^4x \sqrt{-g} \mathcal{L}_m = -\frac{1}{2} \int d^4x \sqrt{-g} (X + 2V(\phi)), \quad (8)$$

with kinetic term  $X \equiv g^{\mu\nu} \partial_\mu \phi \partial_\nu \phi$  and scalar potential  $V(\phi)$ . The variation in this action with respect to the scalar field leads to the field equations

$$\frac{1}{\sqrt{-g}} \partial_\mu (\sqrt{-g} g^{\mu\nu} \partial_\nu \phi) = V_\phi, \quad (9)$$

(where  $V_\phi \equiv dV/d\phi$ ) and to the associated stress-energy tensor

$$T^\mu{}_\nu = g^{\mu\alpha} \partial_\alpha \phi \partial_\nu \phi - \frac{\mathcal{L}_m}{2} \delta^\mu_\nu. \quad (10)$$

We consider next a spatially flat Friedman–Lemaître–Robertson–Walker (FLRW) space–time (For simplicity in this work we do not consider the cases of open and closed universes, although the analysis could also be carried out in such cases following, for instance, the results of [58].), with line element:

$$ds_g^2 \equiv g_{\mu\nu} dx^\mu dx^\nu = -dt^2 + a^2(t) d\vec{x}^2, \quad (11)$$

where  $a(t)$  is the expansion factor and  $d\vec{x}^2 = \delta_{ij} dx^i dx^j$ , with  $i, j = 1 \dots 3$  for the spatial part. From now on, we shall assume  $\phi = \phi(t)$ , the stress-energy tensor (10) reads:

$$T^\mu{}_\nu = \begin{pmatrix} -\frac{1}{2}\dot{\phi}^2 - V & 0 \\ 0 & (\frac{1}{2}\dot{\phi}^2 - V) I_{3 \times 3} \end{pmatrix}. \quad (12)$$

where a dot denotes a derivative with respect to  $t$ , as usual.

From Equation (6) we can conclude that the deformation matrix needs to have a similar algebraic (diagonal) structure as that of the stress-energy tensor of the scalar field, namely

$$\Omega^\mu{}_\nu = \begin{pmatrix} \Omega_+ & 0 \\ 0 & \Omega_- I_{3 \times 3} \end{pmatrix}, \quad (13)$$

where the identity matrix  $I_{3 \times 3}$  represents the spatial sector. Plugging this ansatz and Equation (12) into Equation (6) gives the components of this matrix as:

$$\begin{aligned} \Omega_-^2 &= \left( \lambda + \epsilon \kappa^2 V - \frac{\epsilon \kappa^2 \dot{\phi}^2}{2} \right) \left( \lambda + \epsilon \kappa^2 V + \frac{\epsilon \kappa^2 \dot{\phi}^2}{2} \right) \\ &= (\tilde{\lambda}^2 - \Phi^2) \end{aligned} \quad (14)$$

$$\Omega_+^2 = \frac{\left( \lambda + \epsilon \kappa^2 V - \frac{\epsilon \kappa^2 \dot{\phi}^2}{2} \right)^3}{\left( \lambda + \epsilon \kappa^2 V + \frac{\epsilon \kappa^2 \dot{\phi}^2}{2} \right)} = \frac{(\tilde{\lambda} - \Phi)^3}{(\tilde{\lambda} + \Phi)}, \quad (15)$$

where we have used the shorthand notations

$$\tilde{\lambda} \equiv \lambda + \epsilon \kappa^2 V \quad (16)$$

$$\Phi \equiv \frac{\epsilon \kappa^2 \dot{\phi}^2}{2}. \quad (17)$$

Therefore, we are ready to cast the field Equations (3) for this problem as

$$\epsilon R^\mu{}_\nu(q) = \begin{pmatrix} 1 - \frac{(\tilde{\lambda} + \Phi)}{|\Omega|^{\frac{1}{2}}} & 0 \\ 0 & \left( 1 - \frac{(\tilde{\lambda} - \Phi)}{|\Omega|^{\frac{1}{2}}} \right) \delta_j^i \end{pmatrix}, \quad (18)$$

where the determinant of the deformation matrix reads  $|\Omega|^{\frac{1}{2}} = \Omega_+^{1/2} \Omega_-^{3/2}$ . To compute the left-hand side of the field Equation (18) one can write another line element for the auxiliary metric that is also of the FLRW form:

$$\begin{aligned} ds_q^2 &\equiv q_{\mu\nu} dx^\mu dx^\nu = -dT^2 + \tilde{a}^2(T) d\tilde{x}^2 \\ &= -\Omega_+(t) dt^2 + a^2(t) \Omega_-(t) d\tilde{x}^2, \end{aligned} \quad (19)$$

where, in the second line, we have used the fundamental relation (5) together with the ansatz (13). These gravitational field equations must be supplemented with the scalar field Equation (9) which, in the FLRW background (11), read

$$\ddot{\phi} + 3\frac{\dot{a}}{a}\dot{\phi} + V_\phi = 0. \quad (20)$$

Now, using the fact that in the  $q_{\mu\nu}$  geometry (19), we have the well-known formulas

$$R^t_t \equiv \frac{3}{\tilde{a}} \frac{d^2 \tilde{a}}{dT^2} \quad (21)$$

$$R^i_i \equiv \frac{1}{\tilde{a}} \frac{d^2 \tilde{a}}{dT^2} + \frac{2}{\tilde{a}^2} \left( \frac{d\tilde{a}}{dT} \right)^2, \quad (22)$$

with the relations

$$\frac{d\tilde{a}}{dT} = \frac{1}{\Omega_+^{\frac{1}{2}}} \frac{d}{dt} \left( a \Omega_-^{\frac{1}{2}} \right) \quad (23)$$

$$\frac{d^2 \tilde{a}}{dT^2} = \frac{1}{\Omega_+^{\frac{1}{2}}} \frac{d}{dt} \left[ \frac{1}{\Omega_+^{\frac{1}{2}}} \frac{d}{dt} \left( a \Omega_-^{\frac{1}{2}} \right) \right], \quad (24)$$

it follows that the combination

$$3R^i_i - R^t_t \equiv \frac{6}{\tilde{a}^2} \left( \frac{d\tilde{a}}{dT} \right)^2, \quad (25)$$

can be written as

$$3R^i_i - R^t_t \equiv \frac{6}{\Omega_- \Omega_+} \left[ \frac{1}{a} \frac{d}{dt} \left( a \Omega_-^{\frac{1}{2}} \right) \right]^2, \quad (26)$$

and a little algebra leads to

$$\frac{1}{a} \frac{d}{dt} \left( a \Omega_-^{\frac{1}{2}} \right) = \frac{1}{\Omega_-^{3/2}} \left[ \frac{\dot{a}}{a} (\tilde{\lambda}^2 + 2\Phi^2) + (\tilde{\lambda} + \Phi) \frac{\Phi V_\phi}{\phi} \right],$$

which allows us to find an expression for  $H \equiv \dot{a}/a$

$$H = \frac{1}{(\tilde{\lambda}^2 + 2\Phi^2)} \left[ -(\tilde{\lambda} + \Phi) \frac{\Phi V_\phi}{\phi} \pm \Omega_- \sqrt{\frac{\Omega_+}{3\epsilon}} \left( |\Omega|^{\frac{1}{2}} - (\tilde{\lambda} - 2\Phi) \right) \right]. \quad (27)$$

The square of this quantity is the generalized FLRW equation for EiBI gravity coupled to a scalar field with a potential  $V(\phi)$ . The  $\pm$  signs in front of the square root yield expanding (+) or contracting (−) universes and must be chosen on physical grounds. In the limit  $\epsilon \rightarrow 0$ , the above expression yields

$$H = \pm \sqrt{\frac{\kappa^2(\dot{\phi}^2 + 2V)}{6}}, \quad (28)$$

which recovers the FLRW dynamics of GR coupled to a scalar field.

Note that, from Equation (12), for a scalar field, the energy density  $\rho_\phi$  and pressure  $P_\phi$  are related to the field variables by

$$\rho_\phi \equiv \frac{\dot{\phi}^2}{2} + V \quad (29)$$

$$P_\phi \equiv \frac{\dot{\phi}^2}{2} - V, \quad (30)$$

which allows the quantities inside the functions  $\Omega_\pm$  of Equations (14) and (15) in terms of  $\rho_\phi$  and  $P_\phi$  to be written as

$$\tilde{\lambda} + \Phi = \lambda + \epsilon \kappa^2 \rho_\phi \quad (31)$$

$$\tilde{\lambda} - \Phi = \lambda - \epsilon \kappa^2 P_\phi. \quad (32)$$

### 3. Massless Scalar Fields

To explicitly solve the gravitational and scalar field Equations (18) and (9), we need to specify a form of the scalar potential  $V(\phi)$ . For the sake of simplicity, and to make contact with similar settings in black hole scenarios [59], let us first consider the case of a free scalar field,  $V = 0$ , for which the scalar field equation (20) has a first integral

$$\dot{\phi} = \frac{\phi_0}{a^3(t)}, \quad (33)$$

with  $\phi_0$  an integration constant. This equation is formally the same as in the GR case, although the scale factor implicitly contains the  $\epsilon$ -corrections via the resolution of Equation (27), smoothly reducing to their GR values in the limit  $\epsilon \rightarrow 0$ , as follows from Equation (28).

Since, in this case  $P_\phi = \rho_\phi = \dot{\phi}^2/2$ , the components of the deformation matrix (13) assume the relatively simple form

$$\Omega_- = \left( \lambda^2 - \frac{\rho_\phi^2}{\rho_\epsilon^2} \right)^{\frac{1}{2}}; \quad \Omega_+ = \frac{\left( \lambda - s \frac{\rho_\phi}{\rho_\epsilon} \right)^{3/2}}{\left( \lambda + s \frac{\rho_\phi}{\rho_\epsilon} \right)^{1/2}}, \quad (34)$$

where we have defined the critical density  $\rho_\epsilon = 1/(\kappa^2|\epsilon|)$  and  $s = \pm 1$  denotes the sign of  $\epsilon$ . The corresponding Hubble function takes the form

$$H^2 = \frac{\left( \lambda^2 - \frac{\rho_\phi^2}{\rho_\epsilon^2} \right)^{3/2} \left( \lambda - s \frac{\rho_\phi}{\rho_\epsilon} \right)^2}{3s\epsilon \left( \lambda^2 + 2 \frac{\rho_\phi^2}{\rho_\epsilon^2} \right)^2} \left( \left( \lambda - s \frac{\rho_\phi}{\rho_\epsilon} \right) \sqrt{\lambda^2 - \frac{\rho_\phi^2}{\rho_\epsilon^2}} - \lambda + 2s \frac{\rho_\phi}{\rho_\epsilon} \right). \quad (35)$$

As mentioned before, at low densities as compared to the scale  $\rho_\epsilon$ , this equation recovers the GR expression, which can be solved, leading to the approximate solution  $a(t) = H_0 t^{1/3}$ . The Hubble factor here can be conveniently set to  $H_0^2 = 3\kappa^2 \phi_0^2/2$  to adjust the integration constant  $\phi_0$  in order to reproduce the standard cosmological evolution of GR coupled to a massless scalar field. At higher densities, however, the dynamics strongly depart from that of GR and it is evident that when the energy density of the scalar field approaches its maximum value,  $\rho_\phi = \lambda \rho_\epsilon$ , the Hubble function vanishes. This corresponds to a minimum value of the expansion factor for both branches of solutions  $s = \pm 1$ , but there are two different mechanisms by which the initial Big Bang singularity is avoided, which we will discuss next. For simplicity, from now on, we focus on asymptotically flat configurations,  $\lambda = 1$ .

For the  $s = -1$  branch, at the critical density  $\rho_\phi = \rho_\epsilon$ , the Hubble factor in Equation (35) and its derivative behave as

$$H(\rho_\phi) \approx \pm \frac{2^{7/4}}{3|\epsilon|^{1/2}} \left(1 - \frac{\rho_\phi}{\rho_\epsilon}\right)^{3/4} \quad (36)$$

$$\frac{dH}{d\rho_\phi} \approx \mp \frac{1}{2^{1/4}|\epsilon|^{1/2}\rho_\epsilon \left(1 - \frac{\rho_\phi}{\rho_\epsilon}\right)^{1/4}}. \quad (37)$$

This indicates that at the maximum achievable density,  $\rho_\phi = \rho_\epsilon$ , the Hubble factor vanishes while its derivative goes to infinity. This implies that the universe contracts to a minimum (maximum) value of the expansion factor (energy density), before re-expanding. This is the typical behaviour expected in standard bouncing solutions with a transition from a contracting phase to an expanding one, where the universe could even undergo a sequence of cyclic cosmologies with both phases. In Figure 1, we plot the form of  $H(\rho)$  (blue curves) according to Equation (35) to show that while at late-times (i.e., low densities,  $\rho_\phi \ll \rho_\epsilon$ ) these solutions converge to those of GR (in agreement to Equation (28)), at high densities ( $\rho_\phi/\rho_\epsilon \rightarrow 1$ ) they depart from the standard Big Bang singularity of GR.

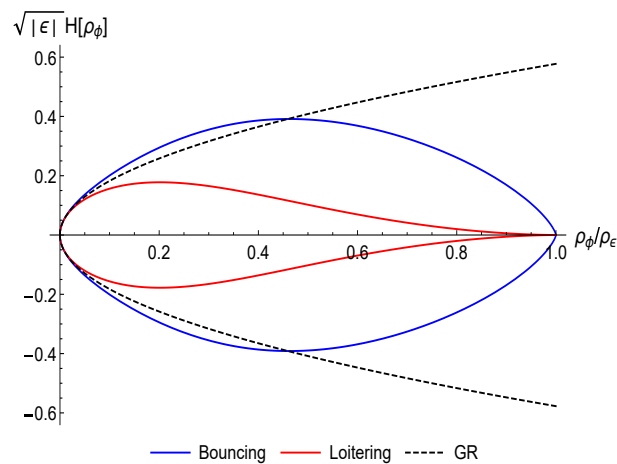


**Figure 1.** Representation of the Hubble function  $\sqrt{|\epsilon|}H(\rho_\phi)$  vs. the energy density for EiBI gravity (solid) and GR (dashed) with massless scalar field as a function of the ratio  $\rho_\phi/\rho_\epsilon$ . Note how the trajectories of the EiBI theory are bounded, while that of GR (dashed black) is open. Bouncing solutions (blue) reach the maximum density forming a  $\pi/2$  angle with the horizontal axis, while the loitering branch (red) reaches it tangentially.

For the  $s = +1$  branch, we find that the evolution of the Hubble factor as we approach the maximum density  $\rho_\phi = \rho_\epsilon$  is given instead by

$$H(\rho_\phi) \approx \pm \frac{2^{3/4}\sqrt{\frac{1}{\epsilon}}\left(1 - \frac{\rho_\phi}{\rho_\epsilon}\right)^{7/4}}{3\sqrt{3}} \quad (38)$$

$$\frac{dH}{d\rho_\phi} \approx \mp \frac{7\sqrt{\frac{1}{\epsilon}}\left(1 - \frac{\rho_\phi}{\rho_\epsilon}\right)^{3/4}}{6\sqrt[4]{2}\sqrt{3}\rho_\epsilon}, \quad (39)$$

which means that the Hubble factor vanishes there as well, but instead of being divergent, its derivative takes a finite value (which is actually zero). This implies that the expansion factor reaches a fixed value  $a(t) = a_m$ , corresponding to an asymptotically Minkowski past, and starts expanding as we move forward in time after some reference time  $t = t_p$ . In Figure 1 we depict this behaviour (red curves) of these so-called loitering solutions, where the qualitative differences with the bouncing solutions are manifest. Again, at late times (low densities), the standard GR evolution is recovered. Therefore, we see that a



free massless scalar field coupled to EiBI gravity is able to yield nonsingular evolutions in both  $s = \pm 1$  branches according to these two mechanisms, something that is not possible within GR.

#### 4. Massive Scalar Field

Let us now consider a massive scalar field with a potential of the form

$$V(\phi) = \frac{1}{2}\mu^2\phi^2, \quad (40)$$

where  $\mu$  is a constant. This choice for the potential, besides being the simplest form, corresponds to the natural mass associated to a canonical scalar field. In this case, the Hubble function (27) develops an explicit dependence on both  $\rho_\phi$  and  $P_\phi$  [to lighten the notation, from now on we shall drop the label  $\phi$  in these quantities] via Equations (31) and (32). Since the resulting expression does not provide any useful insight, we will not write it explicitly here. Instead, for the sake of comparison with the massless case of the previous section, we find it more illustrative to provide a parametric representation of  $H(t)$  versus  $\rho(t)$ . These functions are obtained by numerically integrating the second-order equation for  $\ddot{a}$  that follows from (22), together with its corresponding right-hand side. The result of the integration is used to construct the quantity  $\dot{a}/a$ , which is then compared with the Formula (27) to check the consistency of the numerical integration. Again, we split our discussion of the corresponding results into the  $s = \pm 1$  cases.

In Figures 2 and 3, we show the function  $H(\rho(t))$  from Equation (27) with the help of (14) and (15) particularized to the potential above, for solutions corresponding to several values of the reduced mass  $\sigma \equiv \mu^2/\rho_\epsilon$  in the case  $s = -1$ . The corresponding expansion factors  $a(t)$  (obtained from integrating the previous function  $H$ ) appear in Figure 4, while in Figure 5 we show the function  $\dot{a}(t)$  of those same examples and in Figure 6 their Hubble functions. As one can see from all these plots, the case  $s = -1$  still represents bouncing solutions for all the explored mass range, which goes from  $\sigma \approx 10^{-8}$  up to  $\sigma \approx 0.4$ , with little variation with respect to the massless scenario for masses as high as  $\sigma \approx 10^{-3}$  (see Figure 2). For higher masses, the egg-shaped Hubble function develops a fish-like structure, with asymmetric fins. This asymmetry is also manifest in the contracting branch of the expansion factor (see Figure 4), which becomes increasingly asymmetric as the mass parameter grows from zero. A similar behaviour can be observed in the density profiles of the scalar field depicted in Figure 7.

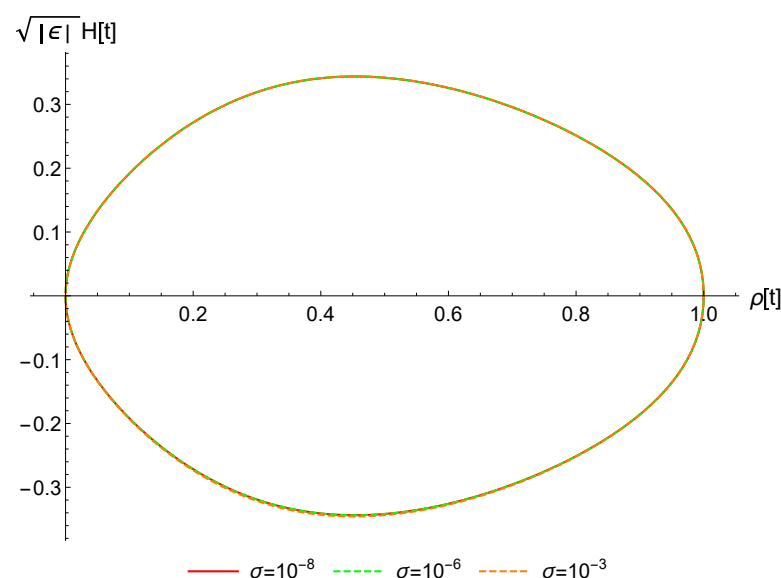


**Figure 2.** Parametric plot of  $\sqrt{|\epsilon|}H(t)$  as a function of  $\rho(t)/\rho_\epsilon$  for small masses when  $s = -1$  (bouncing solutions). The (reduced) mass parameter is taken, such that  $\sigma \equiv \mu^2/\rho_\epsilon$ .



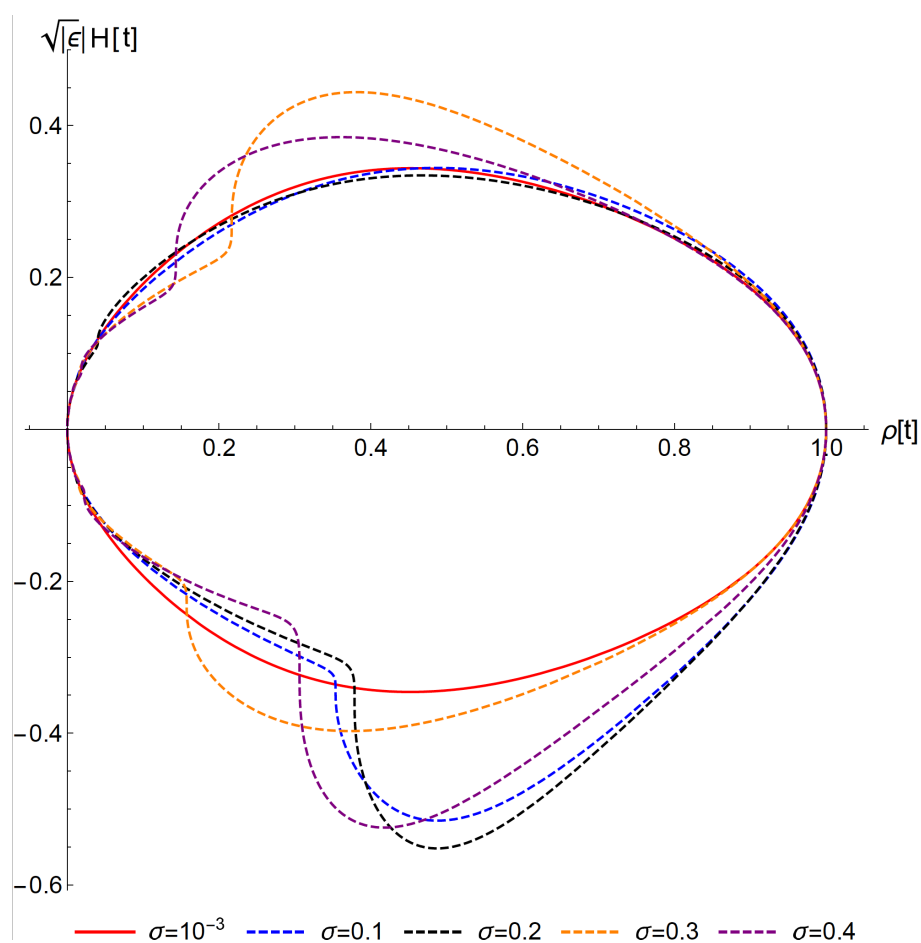


**Figure 3.** Parametric plot of  $\sqrt{|\epsilon|}H(t)$  as a function of  $\rho(t)$  for larger values of the reduced mass  $\sigma \equiv \mu^2/\rho_\epsilon$  when  $s = -1$ . As compared to Figure 2, in this case, the development of fish-like structures is clearly visible as  $\sigma$  grows large enough.

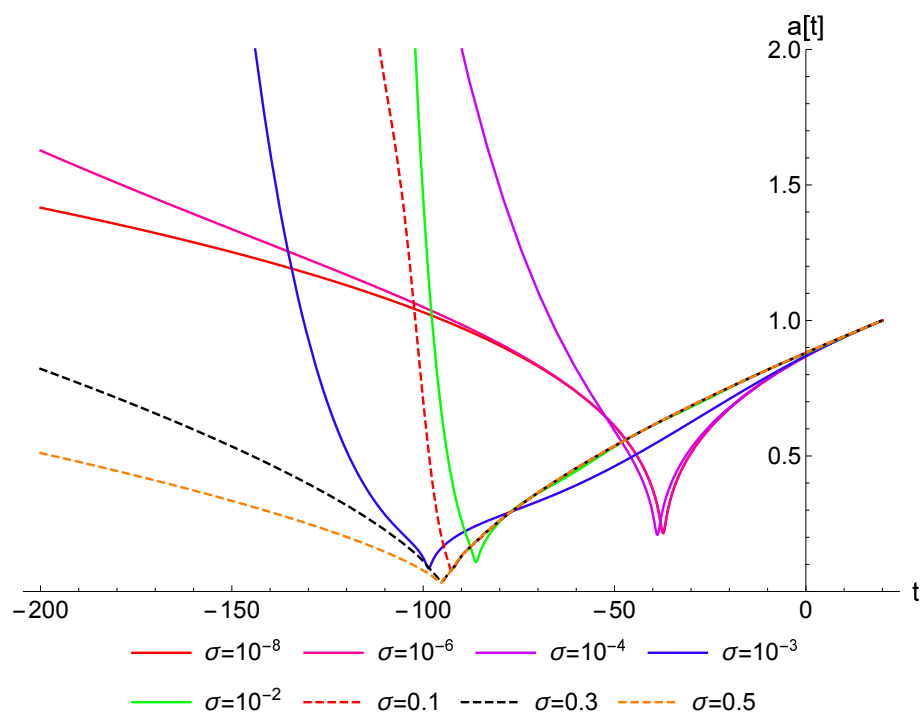


**Figure 4.** Expansion factor  $a(t)$  representing bouncing solutions for various values of the reduced mass parameter  $\sigma \equiv \mu^2/\rho_\epsilon$  when  $s = -1$ .

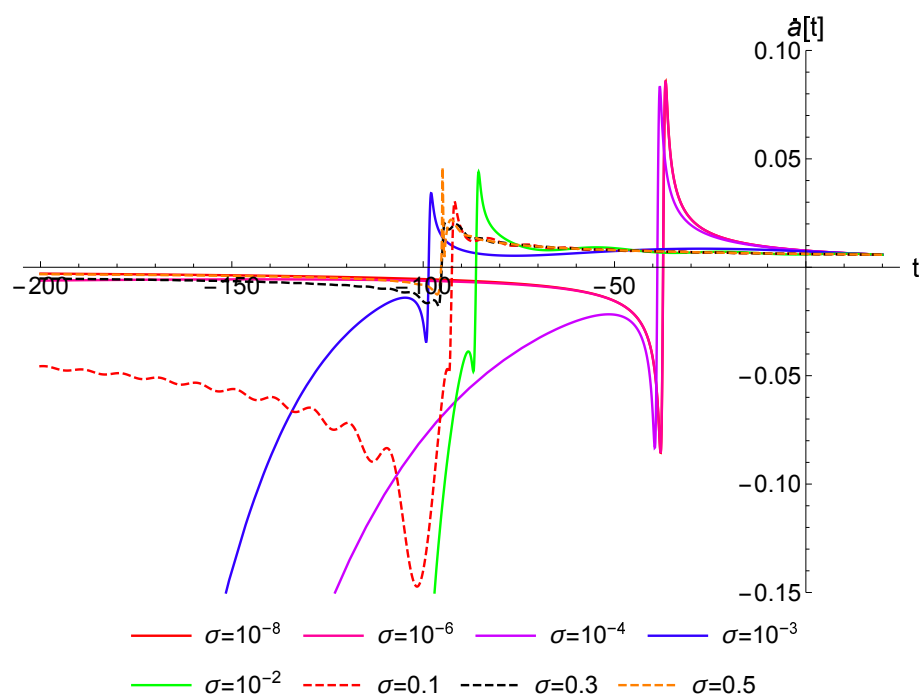


**Figure 5.** Time derivative of the expansion factor representing bouncing solutions for various values of the reduced mass parameter  $\sigma \equiv \mu^2/\rho_\epsilon$ . The colors of the curves are the same as in Figure 4. Note that the blue and magenta curves will bounce at some point and begin a similar growing oscillatory trajectory to the red dashed curve, with this being a generic behavior of all these solutions.

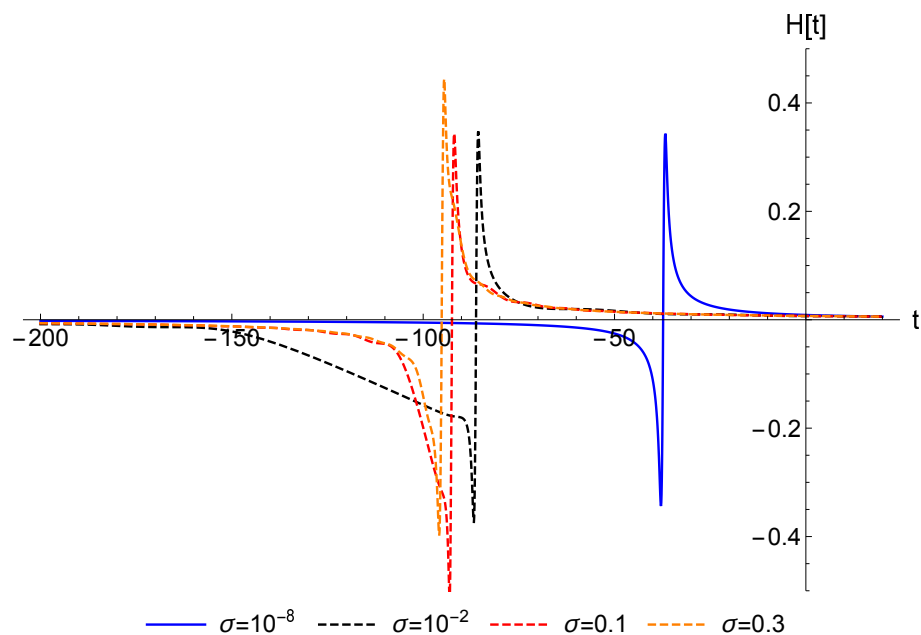


**Figure 6.** Hubble function  $H \equiv \dot{a}/a$  for various values of the reduced mass parameter  $\sigma \equiv \mu^2/\rho_\epsilon$  of the  $s = -1$  case.

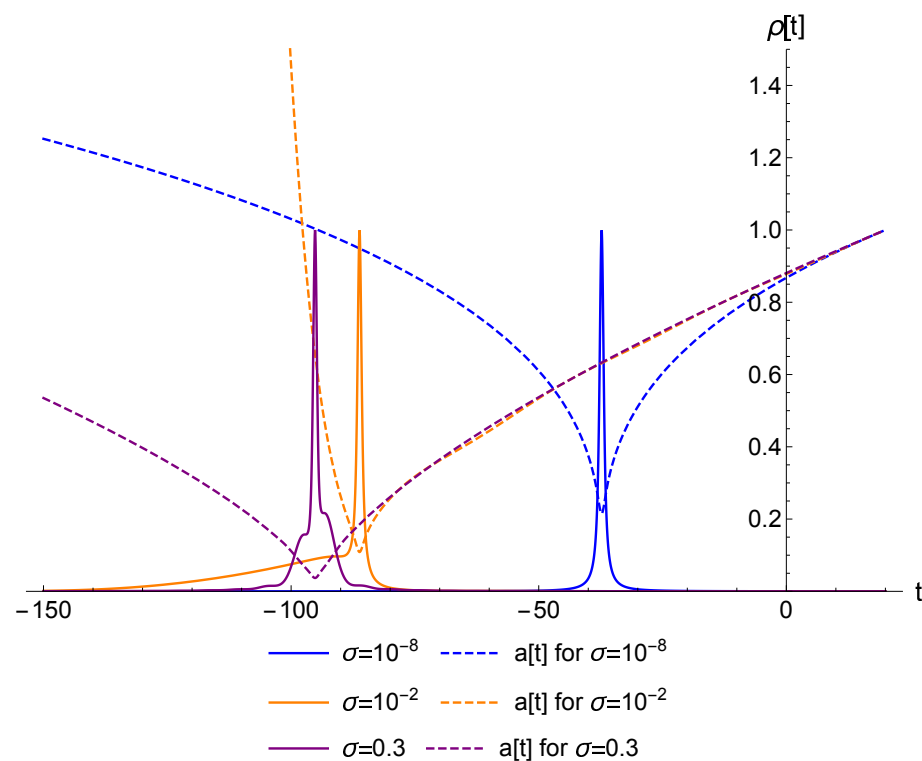


**Figure 7.** Energy density (solid curves) as a function of time superimposed with its corresponding expansion factor  $a(t)$  (dashed curves) for some bouncing solutions of the  $s = -1$  case.

Focusing now on the case with  $s = +1$ , which represents loitering solutions in the massless case, Figure 8 shows that the function  $H(\rho(t))$  is now qualitatively different (compared to Figure 1). Indeed, when  $\sigma = 0$ ,  $H(t)$  never crosses the horizontal axis as one approaches the maximum allowed energy density. However, for  $\sigma \neq 0$ , one either has an expanding branch, which starts from an almost constant  $a(t) = a_m$  initial phase or a contracting phase that ends up in an almost constant final  $a(t) = a_m$ . Now, we observe that *all* solutions develop a bounce at some high density, effectively crossing the axis and establishing a continuous transition from a contracting phase to an expanding one. The loitering phase, with an almost constant  $a(t)$ , may last for a long period after an initial contraction but it will always end up in an expanding branch. This is illustrated in Figure 9, where the blue dashed curve represents a phase with  $a(t)$  almost constant for a long time (very low mass). The orange curve has essentially the same future behaviour as the blue curve, but its loitering phase (almost constant expansion factor) does not last as long, exhibiting a previously contracting phase that abruptly rises. Similar behaviours arise for larger masses, and one verifies that the instabilities in the expansion factor always lead to a bounce, never finding fully collapsed solutions. This is a remarkable property of the EiBI model, since it always avoids the development of singular solutions.

For completeness, the behaviour of  $\dot{a}(t)$  and  $H(t)$  for this case  $s = +1$  are shown in Figures 10 and 11. The corresponding energy density profiles appear in Figures 12 and 13. It is amusing to see how, for low-mass configurations (orange solid curve, for instance), the energy density at early times is very low (large universe with very diluted energy) until it rapidly increases to reach a maximum, where it stays for some time at an almost constant value (loitering phase), with a slight decay (decompression) as we move forward in time. Then, the density suddenly drops again, giving rise to an expanding phase. For larger values of the scalar field mass, this process can be significantly deformed, but the qualitative features remain.

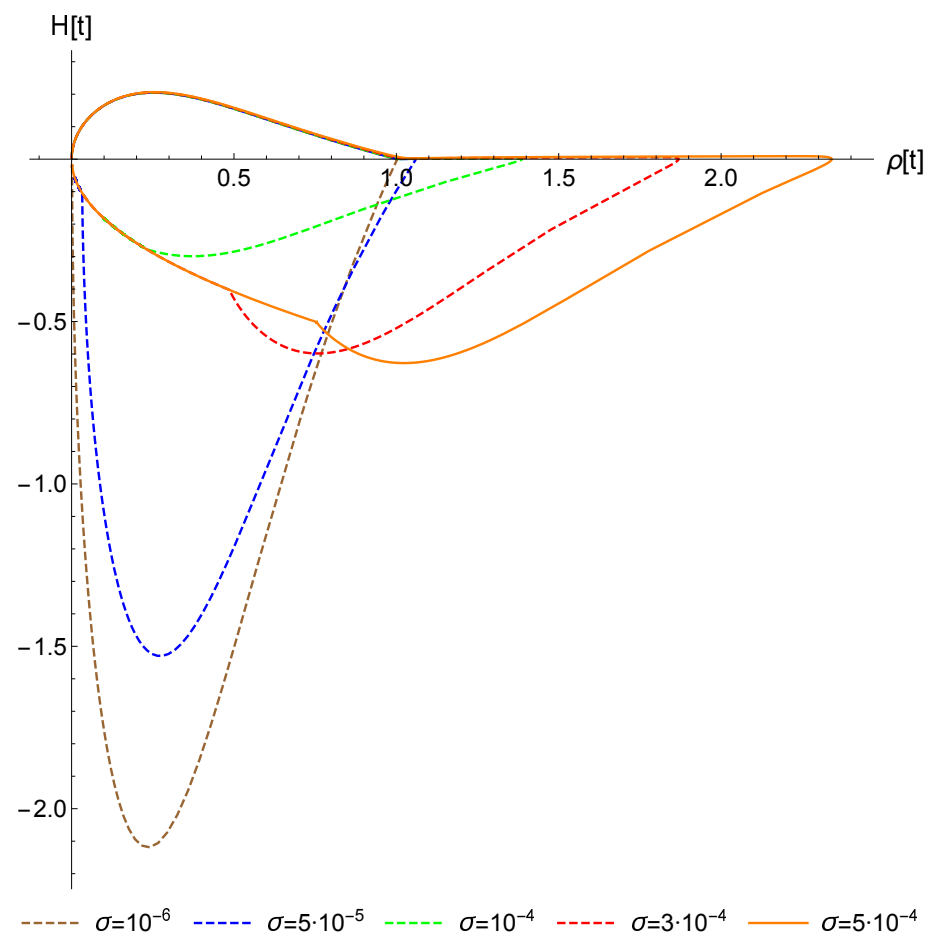


**Figure 8.** Parametric plot of  $H(t)$  as a function of  $\rho(t)$  for small values of the reduced mass  $\sigma$  of the  $s = +1$  case.

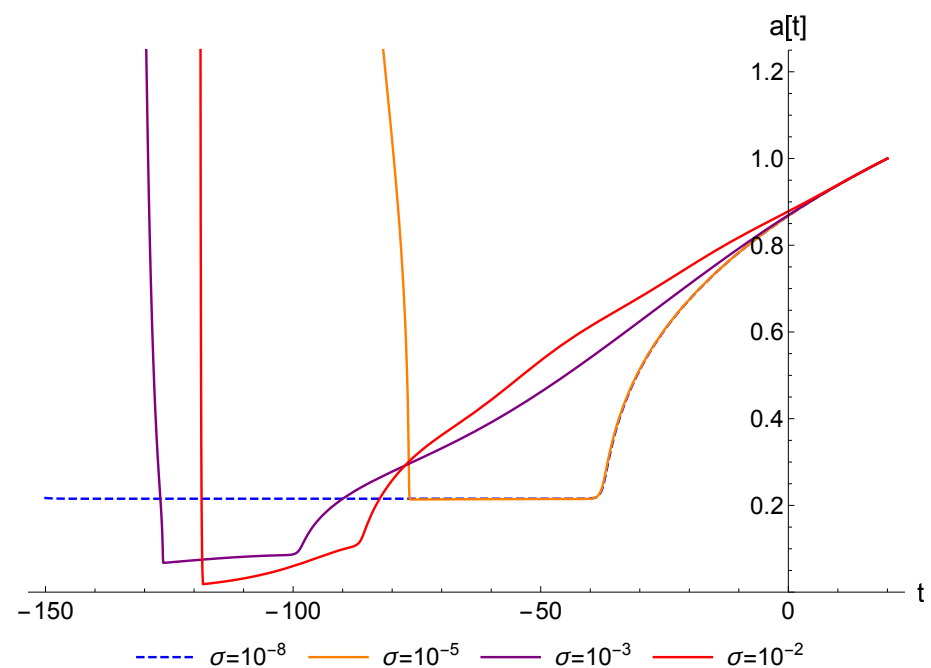


**Figure 9.** Expansion factor representing new bouncing solutions for various values of the reduced mass parameter  $\sigma$  when  $s = +1$ .

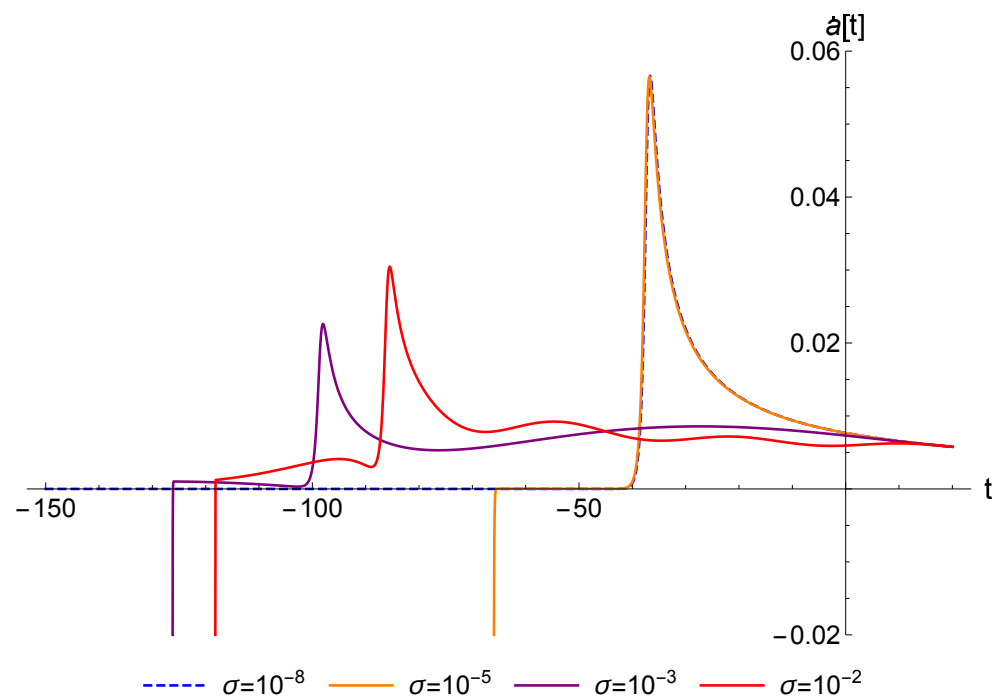


**Figure 10.** Time derivative of the expansion factor representing bouncing solutions for the reduced mass parameter  $\sigma$  when  $s = +1$ .

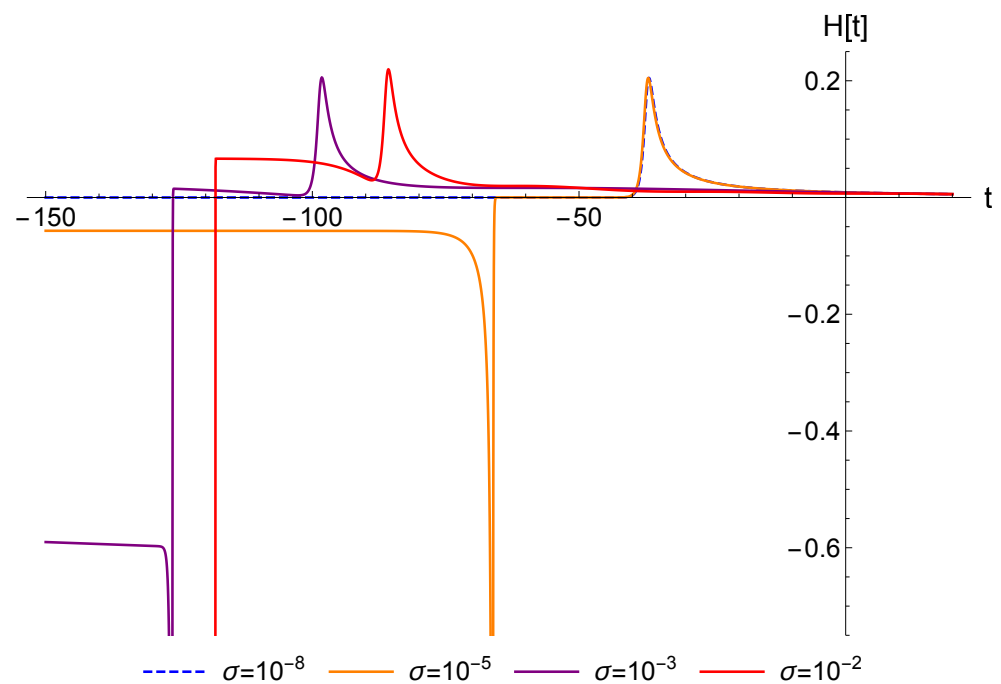


**Figure 11.** Hubble function  $\dot{a}/a$  for various values of the reduced mass parameter  $\sigma$  when  $s = +1$ .

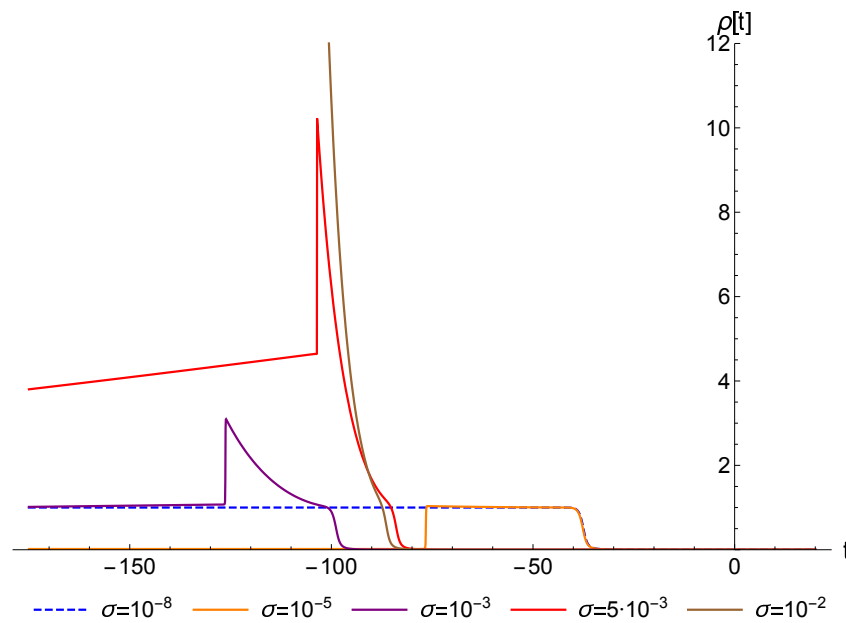


**Figure 12.** Energy density (solid curves) as a function of time superimposed with its corresponding expansion factor  $a(t)$  (dashed curves).

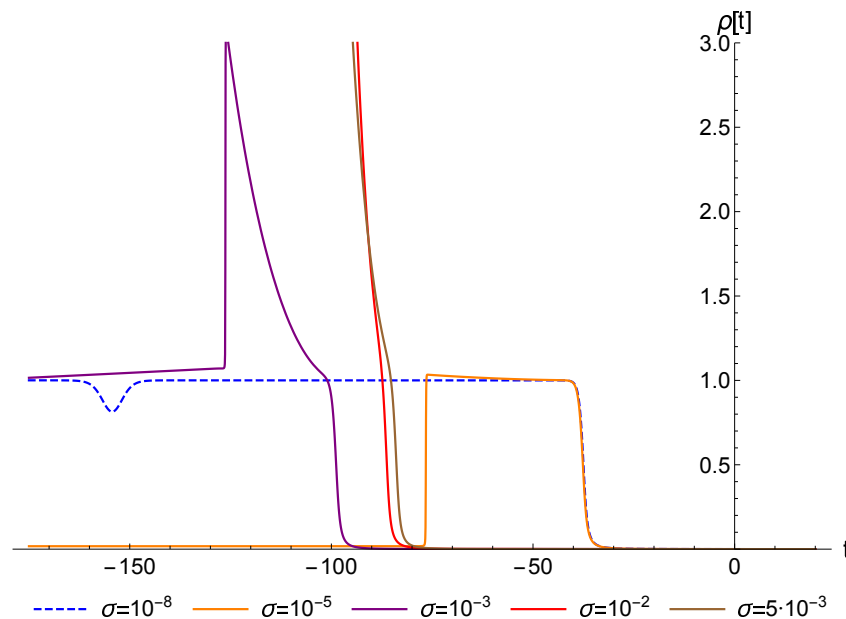


**Figure 13.** Zoom in on the energy density (solid curves) as a function of time superimposed with its corresponding expansion factor  $a(t)$  (dashed curves).

## 5. Observational Constraints

In this section, we shall observationally test the EiBI cosmologies considered in the previous sections by using the latest observational data to constrain the EiBI parameter  $\epsilon$  preventing the singularity in the early Universe.

### 5.1. BBN

In the first sections, we began with the original action with the scalar field inside, and shifted the solution to another frame. This frame, as we showed, removes the singularity of the solution and, for  $\epsilon \rightarrow 0$ , it recovers GR. Here, we put the density of the  $\Lambda$ CDM that produces a solution in the “Einstein frame” that removes the singularity and recovers GR for  $\epsilon \rightarrow 0$ . Using the same procedure for a theory with matter fields  $\rho_m$  in the original frame gives the density:

$$\bar{\rho} = \frac{8(3p\epsilon - 1)^2(3p\epsilon + 1)(2\sqrt{1 - 3p\epsilon}\sqrt{3p\epsilon + 1} - 3\epsilon(p(2\sqrt{1 - 3p\epsilon}\sqrt{3p\epsilon + 1} - 3) - \rho) - 2)}{3\epsilon((3p\epsilon + 1)(3\epsilon(ap' + 4p) - 4) + 3a\epsilon(3p\epsilon - 1)\rho')^2} \quad (41)$$

in the physical frame. For  $\epsilon \rightarrow 0$  the relation gives  $\bar{\rho} = \rho$ , as expected.

To constrain the EiBI parameter  $\epsilon$  we use different measurements from our Universe. The strongest one is from the Big Bang Nucleosynthesis (BBN), where  $z \sim 10^9$ . In principle the condition for the BBN constraint is [60,61]:

$$\left| \frac{\rho_{\text{EiBI}} - \rho_{\Lambda\text{CDM}}}{\rho_{\Lambda\text{CDM}}} \right| < 10\% \quad (42)$$

In this era, the matter dominance is radiation, so we take the density and the pressure to be:

$$\rho = \frac{\Omega_r}{a^4}, \quad p = \frac{\rho}{3}. \quad (43)$$

The density for the EiBI theory gives:

$$\tilde{\Omega} = \frac{(a^4 - \Omega_r\epsilon)^2(a^4 + 3\Omega_r\epsilon)\left(a^4\left(\sqrt{1 - \frac{\Omega_r\epsilon}{a^4}}\sqrt{\frac{3\Omega_r\epsilon}{a^4} + 1} - 1\right) + \Omega_r\epsilon\left(3 - \sqrt{1 - \frac{\Omega_r\epsilon}{a^4}}\sqrt{\frac{3\Omega_r\epsilon}{a^4} + 1}\right)\right)}{3\epsilon(a^8 + 3\Omega_r^2\epsilon^2)^2}. \quad (44)$$

From the condition Equation (42) we get the bound (Recall that restoring dimensions we have  $\epsilon \rightarrow \kappa^2\epsilon$ , which represents the inverse of a matter density. Accordingly, the bound on  $\epsilon$ , which represents a squared length, can be written as  $|\epsilon| \lesssim 5.53 \cdot 10^{-8} \text{ m}^2$ ):

$$|\kappa^2\epsilon| \lesssim 1.03 \cdot 10^{-33}. \quad (45)$$

where we took  $\Omega_r \sim 10^{-4}$ . It is important to note that this bound improves any previous existing bounds on  $\epsilon$  by several orders of magnitude. In fact, the most stringent constraints to date came from elementary particle-scattering experiments [62–64] and implied  $\kappa^2\epsilon \lesssim 1.86 \cdot 10^{-28}$  (or equivalently,  $\epsilon \lesssim 10^{-2} \text{ m}^2$ ).

We now proceed to describe the observational datasets along with the relevant statistics in constraining the model, using the first constraint from the BBN above. The matter fields considered are the dark energy  $\Omega_\Lambda$ , dark matter  $\Omega_m$ , and radiation  $\Omega_r$  components. The corresponding energy density reads

$$\frac{\rho}{\rho_c} = \frac{\Omega_m}{a^3} + \frac{\Omega_r}{a^4} + \Omega_\Lambda. \quad (46)$$

Inserting this equation in the expression of the Hubble factor (27), and assuming a small EiBI parameter,  $|R_{\mu\nu}| \ll \epsilon^{-1}$ , yields the extended Friedman equation:

$$\frac{H^2}{H_0^2} = \frac{\Omega_m}{a^3} + \frac{\Omega_r}{a^4} + \Omega_\Lambda + \epsilon \left( \frac{9\Omega_m^2}{8a^6} + \frac{\Omega_m\Omega_r}{a^7} - \frac{2\Omega_\Lambda\Omega_r}{a^4} \right) + \mathcal{O}(\epsilon^2), \quad (47)$$

where the EiBI corrections to GR solutions are apparent.

## 5.2. Direct Measurements of the Hubble Expansion

Cosmic Chronometers (CC): This dataset exploits the evolution of differential ages of passive galaxies at different redshifts to directly constrain the Hubble parameter [65]. We use the uncorrelated 30 CC measurements of  $H(z)$  discussed in [66–69]. The corresponding  $\chi_H^2$  function reads:

$$\chi_H^2 = \sum_{i=1}^{30} \left( \frac{H_i - H_{\text{pred}}(z_i)}{\Delta H_i} \right)^2, \quad (48)$$



where  $H_i$  is the observed Hubble rates at redshift  $z_i$  ( $i = 1, \dots, N$ ) and  $H_{pred}$  is the predicted one from the model.

### 5.3. Standard Candles

As Standard Candles (SC), we use measurements of the Pantheon type Ia supernova [70], that were collected in [71], as well as quasars [72] and gamma ray bursts [73]. The model parameters are fitted by comparing the observed  $\mu_i^{obs}$  value to the theoretical  $\mu_i^{th}$  value of the distance moduli, which are the logarithms:

$$\mu = m - M = 5 \log_{10}(D_L) + \mu_0, \quad (49)$$

where  $m$  and  $M$  are the apparent and absolute magnitudes and  $\mu_0 = 5 \log(H_0^{-1}/Mpc) + 25$  is the nuisance parameter that has been marginalized. The luminosity distance is defined by

$$D_L(z) = \frac{c}{H_0} (1+z) \int_0^z \frac{dz'}{E(z')}, \quad (50)$$

(here  $\Omega_k = 0$ , i.e., a flat space-time and  $E(z)$  is the dimensionless Hubble parameter). For the SNIa data the covariance matrix is not diagonal and the distance modulus is given as  $\mu_i = \mu_{B,i} - \mathcal{M}$ , where  $\mu_{B,i}$  is the apparent magnitude at maximum in the rest frame for redshift  $z_i$  and  $\mathcal{M}$  is treated as a universal free parameter, quantifying various observational uncertainties [70]. Following standard lines, the chi-square function of the standard candles is given by

$$\chi_{SC}^2(\phi_s^v) = \mu_s C_{s,cov}^{-1} \mu_s^T, \quad (51)$$

where  $\mu_s = \{\mu_1 - \mu_{th}(z_1, \phi^v), \dots, \mu_N - \mu_{th}(z_N, \phi^v)\}$  and the subscript 's' denotes SNIa and QSOs.

### 5.4. Baryon Acoustic Oscillations

We use uncorrelated datapoints from different Baryon Acoustic Oscillations (BAO). BAO are a direct consequence of the strong coupling between photons and baryons in the pre-recombination epoch. After the decoupling of photons, the over densities in the baryon fluid evolved and attracted more matter, leaving an imprint in the two-point correlation function of matter fluctuations with a characteristic scale of around  $r_d \approx 147$  Mpc that can be used as a standard ruler and to constrain cosmological models. Studies of the BAO feature in the transverse direction provide a measurement of  $D_H(z)/r_d = c/H(z)r_d$ , with the comoving angular diameter distance [74,75]:

$$D_M = \int_0^z \frac{c dz'}{H(z')}. \quad (52)$$

The angular diameter distance  $D_A = D_M/(1+z)$  and the quantity  $D_V(z)/r_d$  with

$$D_V(z) \equiv [z D_H(z) D_M^2(z)]^{1/3} \quad (53)$$

are a combination of the BAO peak coordinates above. The surveys provide the values of the measurements at some effective redshift. We employ the BAO datapoints collected in [76] from [77–88], in the redshift range  $0.106 < z < 2.34$ . The BAO scale is set by the sound horizon at the drag epoch  $z_d \approx 1060$  when photons and baryons decouple. In our analysis, we used  $r_d$  as an independent parameter.

The BAO data represent the absolute distance measurements in the Universe. From the measurements of correlation function or power spectrum of a large-scale structure, we can use the BAO signal to estimate the distance scales at different redshifts. In practice,

the BAO data are analyzed based on a fiducial cosmology and the sound horizon at drag epoch. We calculate the redshift of the drag epoch as:

$$z_d = \frac{1291\omega_m^{0.251}}{1 + 0.659\omega_m^{0.828}}[1 + b_1\omega_b^{b_2}], \quad (54)$$

where

$$b_1 = 0.313\omega_m^{-0.419}[1 + 0.607\omega_m^{0.674}], \quad (55)$$

$$b_2 = 0.238\omega_m^{0.223}. \quad (56)$$

The uncorrelation of this dataset yields the corresponding  $\chi^2$ :

$$\chi_{BAO}^2 = \sum_{i=1}^{17} \left( \frac{D_i - D_{pred}(z_i)}{\Delta D_i} \right)^2, \quad (57)$$

where  $D_i$  is the observed distant module rates at redshift  $z_i$  ( $i = 1, \dots, N$ ) and  $D_{pred}$  is the predicted one from the model.

### 5.5. CMB Distant Priors

We use the CMB distant priors that based on the latest CMB measurements [2]. Its contribution in the likelihood analysis is expressed in terms of the compressed form with CMB shift parameters:

$$R \equiv \sqrt{\Omega_m H_0^2 r(z_*)}/c, \quad (58)$$

$$l_a \equiv \pi r(z_*)/r_s(z_*), \quad (59)$$

where  $r_s(z)$  is the comoving sound horizon at redshift  $z$ , and  $z_*$  is the redshift to the photon-decoupling surface. These two CMB shift parameters, together with  $\omega_b = \Omega_b h^2$  and spectral index of the primordial power spectrum  $n_s$ , can give an efficient summary of CMB data for the dark energy constraints.

The comoving sound horizon is given by

$$r_s(z) = \frac{c}{H_0} \int_0^a \frac{da'}{\sqrt{3(1 + \bar{R}_b a') a'^4 E^2(z')}}. \quad (60)$$

The radiation term in the expression of  $E(z)$  for the CMB data analysis should not be ignored. It can be determined by the matter–radiation equality relation  $\Omega_r = \Omega_m/(1 + z_{eq})$ , and  $z_{eq} = 2.5 \times 10^4 \omega_m (T_{CMB}/2.7K)^{-4}$ , where  $\omega_m = \Omega_m h^2$ . The sound speed is  $c_s = 1/\sqrt{3(1 + \bar{R}_b a)}$ , with  $\bar{R}_b a = 3\rho_b/(4\rho_r)$ , and  $\bar{R}_b = 31,500\omega_b (T_{CMB}/2.7K)^{-4}$ . We assume the CMB temperature  $T_{CMB} = 2.7255K$ . The redshift  $z_*$  can be calculated by the fitting formula:

$$z_* = 1048[1 + 0.00124\omega_b^{-0.738}][1 + g_1\omega_m^{g_2}], \quad (61)$$

where

$$g_1 = \frac{0.0783\omega_b^{-0.238}}{1 + 39.5\omega_b^{0.763}}, \quad g_2 = \frac{0.560}{1 + 21.1\omega_b^{1.81}}. \quad (62)$$

### 5.6. Direct Detection of the Hubble Parameter

We include the latest measurement of the Hubble parameter:

$$H_0 = (73.2 \pm 1.3) \text{ km/s/Mpc} \quad (63)$$

reported by [89]. The measurement presents an expanded sample of 75 Milky Way Cepheids with Hubble Space Telescope (HST) photometry and Gaia EDR3 parallaxes,

which uses the extragalactic distance ladder to recalibrate and refine the determination of the Hubble constant. The combination is related via the relation

$$\chi_{Hub}^2 = \left( \frac{H_0 - 73.2}{1.3} \right)^2. \quad (64)$$

The  $\chi_{Hub}^2$  estimates the deviation from the latest measurement of the Hubble constant.

### 5.7. Joint Analysis and Model Selection

In order to perform a joint statistical analysis of 4 cosmological probes, we need to use the total likelihood function; consequently, the  $\chi_{tot}^2$  expression is given by

$$\chi_{tot}^2 = \chi_{BBN}^2 + \chi_{CMB}^2 + \chi_H^2 + \chi_{SC}^2 + \chi_{BAO}^2 + \chi_{Hub}^2. \quad (65)$$

In order to perform a joint statistical analysis of these four cosmological probes, we need to use the total likelihood function. Regarding the problem of likelihood maximization, we use an affine-invariant Markov Chain Monte Carlo sampler [90], as was implemented within the open-source packaged *Polychord* [91] with the *GetDist* package [92] to present the results. The prior we choose has a uniform distribution, where  $\Omega_m \in [0; 1]$ ,  $\Omega_\Lambda \in [0; 1 - \Omega_m]$ ,  $H_0 \in [50; 100]$  Km/sec/Mpc. For the EiBI parameter  $\epsilon$ , we set the range  $|\kappa^2 \epsilon| \in [0; 10^{-33}]$ .

The posterior distribution of  $H_0$  vs. the EiBI parameter  $\epsilon$  is presented in Figure 14 and 15. The Hubble parameter is  $H_0 = 64.99 \pm 0.556$  km/sec/Mpc, which is between the Planck estimation of the Hubble function [2] and the latest SH0ES measurement [89]. The dark-matter component is  $\Omega_m = 0.291 \pm 0.0074$ , and the dark energy component is  $\Omega_\Lambda = 0.689 \pm 0.0084$ . The fit for the EiBI parameter gives  $\kappa^2 \epsilon = (4.764 \pm 3.074) \cdot 10^{-33}$ . We point out that the value of  $\epsilon = 0$  (which corresponds to GR) is very close to the mean value. Therefore, for  $|\epsilon| \lesssim (5.76 \pm 3.53) \cdot 10^{-8} \text{m}^2$  the theory is able to fit to the data while being able to successfully remove the Big Bang singularity. We point out again that this improves the previous strongest constraints for EiBI gravity's parameter, as obtained from particle physics experiments, by several orders of magnitude [62–64].

We finally point out that from the Bayes factor difference between the models that reads  $\Delta B_{ij} = 0.51$ , we get an indistinguishable difference for the  $\Lambda$ CDM model. Therefore, EiBI gravity with this constraint on its parameter when coupled to a scalar, yields very similar properties for the  $\Lambda$ CDM model, but prevents the initial singularity.

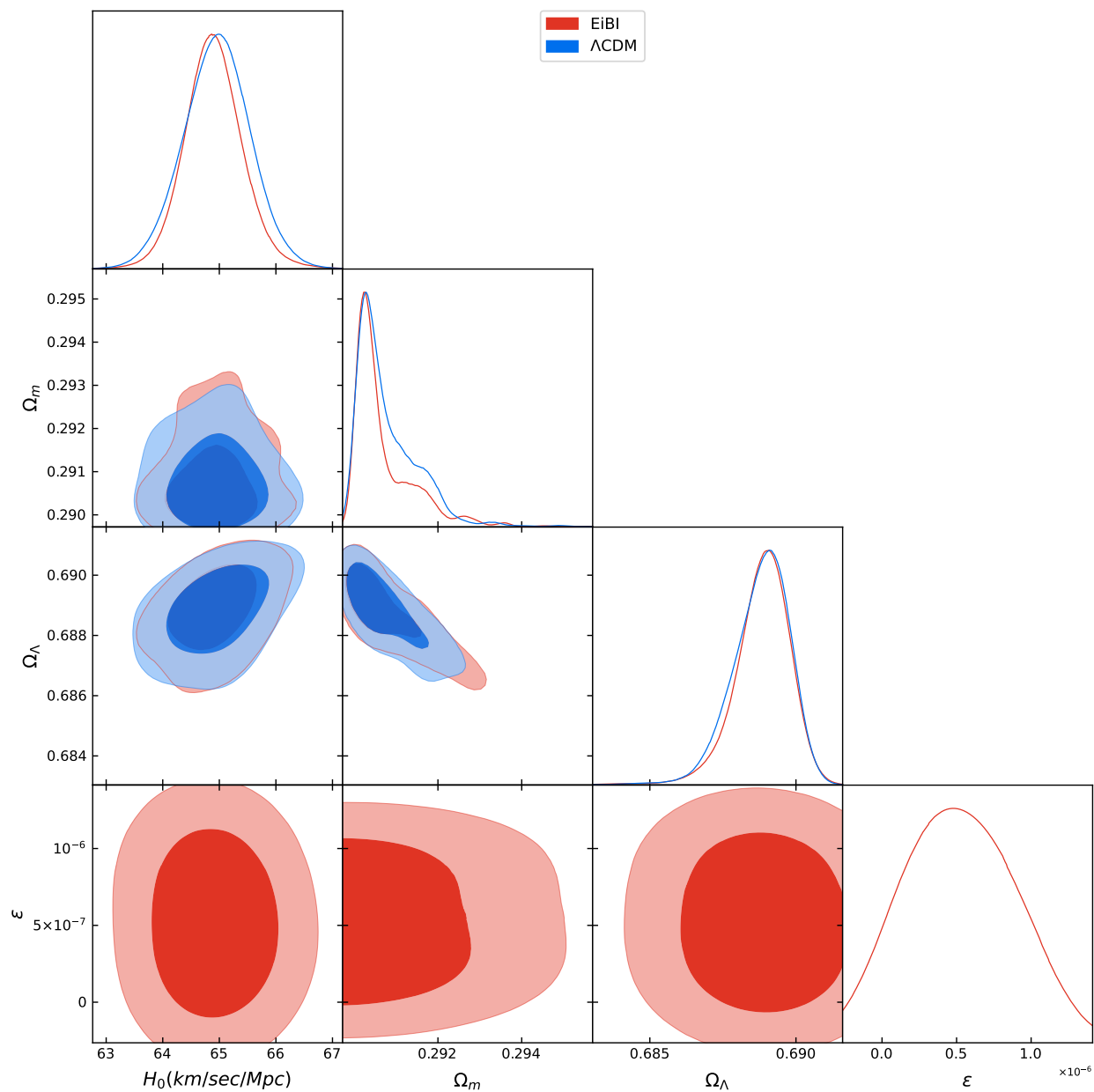


**Figure 14.** The posterior distribution for the simplest case of the EiBI and for  $\Lambda$ CDM model (blue curve). The ratios of the matter density  $\Omega_m$ , dark energy  $\Omega_\Lambda$ . The final results for cosmological parameters for the EiBI and the  $\Lambda$ CDM models are summarized Table 1. In order to compare the models, we calculate the Bayes factor.

**Table 1.** The cosmological parameters for EiBI gravity as compared to  $\Lambda$ CDM, and the corresponding bound on  $\epsilon$ .

Model	$H_0$ (Km/sec/Mpc)	$\Omega_m$	$\Omega_\Lambda$	$\epsilon(10^{-8})$	$\Delta B_{ij}$
EiBI	$64.99 \pm 0.556$	$0.291 \pm 0.0074$	$0.689 \pm 0.0084$	$(5.76 \pm 3.53)$	0.51
$\Lambda$ CDM	$64.94 \pm 0.525$	$0.291 \pm 0.008$	$0.6891 \pm 0.00865$	-	-

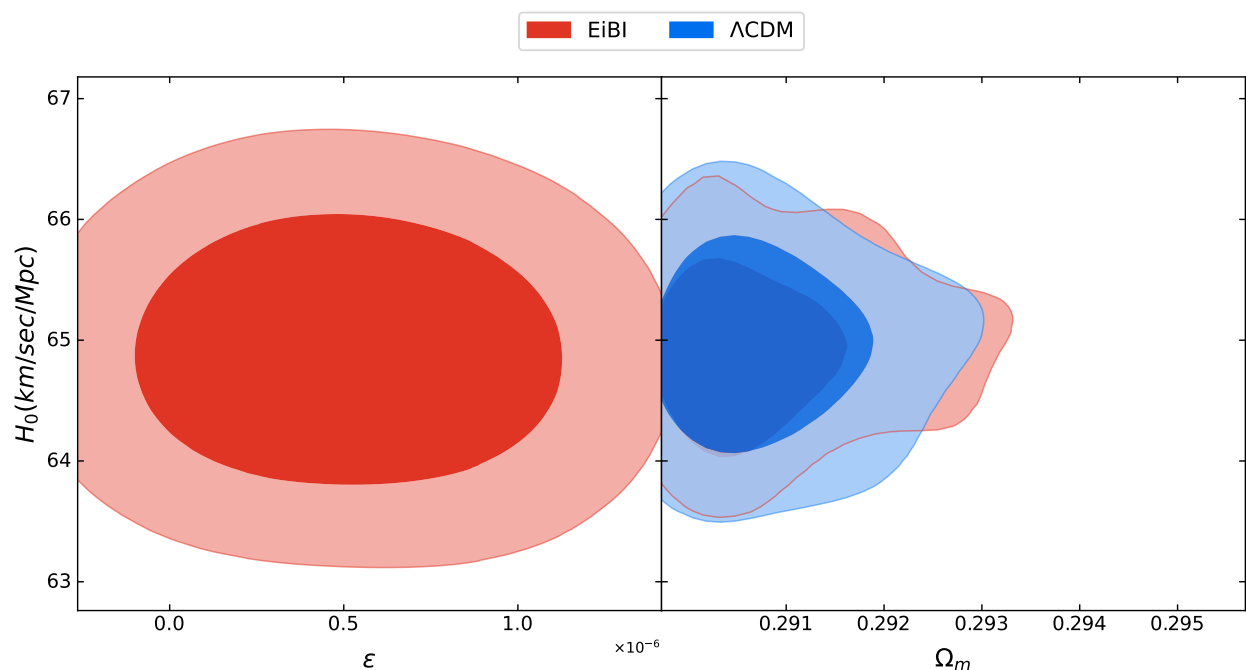


**Figure 15.** The posterior distribution for the Hubble parameter  $H_0$  vs. the EiBI parameter  $\epsilon$ .

## 6. Conclusions and Discussion

In this paper, we analyzed homogeneous and isotropic cosmological solutions in the context of Eddington-inspired Born–Infeld gravity coupled to a single scalar field. In the massless case, we discussed the existence and properties of such solutions by direct resolution of the modified gravitational field equations, which depend on the sign of the EiBI parameter. For the bouncing solutions ( $s = -1$ ), one finds that, at the maximum achievable density of the scalar field, the expansion factor gets to a minimum non-vanishing value (vanishing Hubble factor) undergoing a transition from a contracting phase to an expanding one (or vice versa). In the loitering solutions ( $s = +1$ ) the cosmological evolution starts from an asymptotically Minkowski past with a minimum constant value of the expansion factor, such that, at a given time, a canonical cosmological expansion phase is triggered. These results are consistent with the expectancy raised in the seminal paper [35] and the numerical evidence found in more recent works [93] when considering perfect fluids as the matter source.

Although the massless case was known to have only two types of solutions, namely, bouncing and loitering, some kind of instability was expected for the loitering case beyond the massless scenario. It was not previously known if they would lead to singular solutions or if they would remain nonsingular. Our analysis suggests that the model is absolutely robust against singularities and that the loitering case gives rise to a new type of solution in which an unstable Minkowskian phase (almost constant expansion factor) is possible between a contraction phase and an expansion phase. The duration of this Minkowskian period (see Figure 9) depends on model parameters and the initial conditions. No singular solutions are found in our analysis, in either the massless or the massive case. All the nonsingular solutions recover the late-time GR cosmological evolution.

Getting into the details, for the  $s = -1$  (bouncing) branch we found that, for low masses, the solutions closely resemble the behaviour of those of the massless case. However, for masses above a certain threshold, the parametric representation of the Hubble function versus the energy density develops a kind of fish-like asymmetric fins at certain time in the cosmological evolution, a feature that is not present in the massless case (compare Figure 1 with Figures 2 and 3). The  $s = +1$  (loitering) branch also exhibits unusual features, showing that, during the loitering (almost Minkowskian) phase, the energy density can grow significantly while the Hubble function remains close to zero and positive (see

Figure 8). This represents a kind of intermediate state in a continuous transition from a contracting phase to a final expansion one. This behaviour is triggered by the energy density stored in the massive scalar field, whose drop marks the end of the loitering phase and the beginning of the expansion phase (see Figures 12 and 13).

To conclude, the results obtained in this paper further support the effectiveness of EiBI gravity to remove singularities in cosmological and astrophysical scenarios when coupled to different matter sources. In the present scenario with scalar fields, this can be performed while being consistent with the latest cosmological observations, provided that the EiBI parameter is kept roughly within  $|\epsilon| \lesssim 5 \cdot 10^{-8} \text{ m}^2$ . One important aspect of the solutions that are not tackled here is whether they are stable under tensorial perturbations. We point out that, in the present case, the equation of state is of the form  $\omega = \omega(t)$ , since the energy density and the pressure of the scalar field (in the massive case) are not trivially related. In turn, this should have an impact on the behaviour of the quantities that are prone to the development of instabilities in the tensorial perturbations equation, such as the sound speed [93,94]. Therefore, one would need to carry out such an analysis to further support the feasibility of this theory and their associated solutions to replace the Big Bang singularity with observationally viable nonsingular cosmologies.

**Author Contributions:** Writing—original draft preparation, D.B., G.J.O. and D.R.-G.; writing—review and editing, D.B., G.J.O. and D.R.-G. All authors contributed equally to the manuscript. All authors have read and agreed to the published version of the manuscript.

**Funding:** D.B. gratefully acknowledges the support from the Blavatnik and the Rothschild fellowship. G.J.O. is no longer funded by the Ramon y Cajal contract RYC-2013-13019 (Spain) because he became permanent. D.R.-G. is funded by the *Atracción de Talento Investigador* programme of the Comunidad de Madrid (Spain) No. 2018-T1/TIC-10431, and acknowledges further support from the Ministerio de Ciencia, Innovación y Universidades (Spain) project No. PID2019-108485GB-I00/AEI/10.13039/501100011033, and the FCT projects No. PTDC/FIS-PAR/31938/2017 and PTDC/FIS-OUT/29048/2017. This work is supported by the Spanish Grant FIS2017-84440-C2-1-P funded by MCIN/AEI/10.13039/501100011033 “ERDF A way of making Europe”, Grant PID2020-116567GB-C21 funded by MCIN/AEI/10.13039/501100011033, the project PROMETEO/2020/079 (Generalitat Valenciana), the project i-COOPB20462 (CSIC) and the Edital 006/2018 PRONEX (FAPESQ-PB/CNPQ, Brazil, Grant 0015/2019). This article is based on work from COST Action CA18108, supported by COST (European Cooperation in Science and Technology).

**Acknowledgments:** D.B. thanks the Department of Theoretical Physics of the Complutense University of Madrid for their hospitality during the elaboration of this work.

**Conflicts of Interest:** The authors declare no conflict of interest.

## References

1. Amendola, L. Cosmology and fundamental physics with the Euclid satellite. *Living Rev. Relativ.* **2013**, *16*, 6. [CrossRef]
2. Aghanim, N. Planck 2018 results. VI. Cosmological parameters. *Astron. Astrophys.* **2020**, *641*, A6. [CrossRef]
3. Starobinsky, A.A. Spectrum of relict gravitational radiation and the early state of the universe. *JETP Lett.* **1979**, *30*, 682–685.
4. Starobinsky, A.A. A New Type of Isotropic Cosmological Models Without Singularity. *Phys. Lett.* **1980**, *91B*, 99–102. [CrossRef]
5. Guth, A.H. The Inflationary Universe: A Possible Solution to the Horizon and Flatness Problems. *Phys. Rev.* **1981**, *D23*, 347–356. [CrossRef]
6. Albrecht, A.; Steinhardt, P.J. Cosmology for Grand Unified Theories with Radiatively Induced Symmetry Breaking. *Phys. Rev. Lett.* **1982**, *48*, 1220–1223. [CrossRef]
7. Mukhanov, V.F.; Chibisov, G.V. Quantum Fluctuations and a Nonsingular Universe. *JETP Lett.* **1981**, *33*, 532–535.
8. Guth, A.H.; Pi, S.Y. Fluctuations in the New Inflationary Universe. *Phys. Rev. Lett.* **1982**, *49*, 1110–1113. [CrossRef]
9. Linde, A.D. A New Inflationary Universe Scenario: A Possible Solution of the Horizon, Flatness, Homogeneity, Isotropy and Primordial Monopole Problems. *Phys. Lett.* **1982**, *108B*, 389–393. [CrossRef]
10. Barrow, J.D.; Cotsakis, S. Inflation and the Conformal Structure of Higher Order Gravity Theories. *Phys. Lett.* **1988**, *B214*, 515–518. [CrossRef]
11. Barrow, J.D. The Premature Recollapse Problem in Closed Inflationary Universes. *Nucl. Phys. B* **1988**, *296*, 697–709. [CrossRef]
12. Elizalde, E.; Nojiri, S.; Odintsov, S.D.; Saez-Gomez, D.; Faraoni, V. Reconstructing the universe history, from inflation to acceleration, with phantom and canonical scalar fields. *Phys. Rev. D* **2008**, *77*, 106005. [CrossRef]



13. Ratra, B.; Peebles, P.J.E. Cosmological Consequences of a Rolling Homogeneous Scalar Field. *Phys. Rev.* **1988**, *D37*, 3406. [[CrossRef](#)] [[PubMed](#)]
14. Caldwell, R.R.; Dave, R.; Steinhardt, P.J. Cosmological imprint of an energy component with general equation of state. *Phys. Rev. Lett.* **1998**, *80*, 1582–1585. [[CrossRef](#)]
15. Kehayias, J.; Scherrer, R.J. New generic evolution for  $k$ -essence dark energy with  $w \approx -1$ . *Phys. Rev.* **2019**, *D100*, 023525. [[CrossRef](#)]
16. Oikonomou, V.K.; Chatzarakis, N. The Phase Space of  $k$ -Essence  $f(R)$  Gravity Theory. *Nucl. Phys.* **2020**, *B956*, 115023. [[CrossRef](#)]
17. Chakraborty, A.; Ghosh, A.; Banerjee, N. Dynamical systems analysis of a  $k$ -essence model. *Phys. Rev.* **2019**, *D99*, 103513. [[CrossRef](#)]
18. Babichev, E.; Ramazanov, S.; Vikman, A. Recovering  $P(X)$  from a canonical complex field. *arXiv* **2018**, arXiv:1807.10281.
19. Zlatev, I.; Wang, L.M.; Steinhardt, P.J. Quintessence, cosmic coincidence, and the cosmological constant. *Phys. Rev. Lett.* **1999**, *82*, 896–899. [[CrossRef](#)]
20. Caldwell, R.R. A Phantom menace? *Phys. Lett.* **2002**, *B545*, 23–29. [[CrossRef](#)]
21. Chiba, T.; Okabe, T.; Yamaguchi, M. Kinetically driven quintessence. *Phys. Rev.* **2000**, *D62*, 023511. [[CrossRef](#)]
22. Bento, M.C.; Bertolami, O.; Sen, A.A. Generalized Chaplygin gas, accelerated expansion and dark energy matter unification. *Phys. Rev.* **2002**, *D66*, 043507. [[CrossRef](#)]
23. Tsujikawa, S. Quintessence: A Review. *Class. Quant. Grav.* **2013**, *30*, 214003. [[CrossRef](#)]
24. Hu, W.; Barkana, R.; Gruzinov, A. Cold and fuzzy dark matter. *Phys. Rev. Lett.* **2000**, *85*, 1158–1161. [[CrossRef](#)] [[PubMed](#)]
25. Anagnostopoulos, F.K.; Benisty, D.; Basilakos, S.; Guendelman, E.I. Dark energy and dark matter unification from dynamical space time: Observational constraints and cosmological implications. *JCAP* **2019**, *1906*, 003. [[CrossRef](#)]
26. Benisty, D.; Guendelman, E.; Haba, Z. Unification of dark energy and dark matter from diffusive cosmology. *Phys. Rev.* **2019**, *D99*, 123521. [[CrossRef](#)]
27. Benisty, D.; Guendelman, E.I. Unified dark energy and dark matter from dynamical spacetime. *Phys. Rev.* **2018**, *D98*, 023506. [[CrossRef](#)]
28. Benisty, D.; Guendelman, E.I. Interacting Diffusive Unified Dark Energy and Dark Matter from Scalar Fields. *Eur. Phys. J.* **2017**, *C77*, 396. [[CrossRef](#)]
29. Senovilla, J.M.M.; Garfinkle, D. The 1965 Penrose singularity theorem. *Class. Quant. Grav.* **2015**, *32*, 124008. [[CrossRef](#)]
30. De Felice, A.; Tsujikawa, S.  $f(R)$  theories. *Living Rev. Relativ.* **2010**, *13*, 3. [[CrossRef](#)] [[PubMed](#)]
31. Capozziello, S.; De Laurentis, M. Extended Theories of Gravity. *Phys. Rep.* **2011**, *509*, 167–321. [[CrossRef](#)]
32. Nojiri, S.; Odintsov, S.D.; Oikonomou, V.K. Modified Gravity Theories on a Nutshell: Inflation, Bounce and Late-time Evolution. *Phys. Rep.* **2017**, *692*, 1–104. [[CrossRef](#)]
33. Heisenberg, L. A systematic approach to generalisations of General Relativity and their cosmological implications. *Phys. Rep.* **2019**, *796*, 1–113. [[CrossRef](#)]
34. Bull, P. Beyond  $\Lambda$ CDM: Problems, solutions, and the road ahead. *Phys. Dark Univ.* **2016**, *12*, 56–99. [[CrossRef](#)]
35. Banados, M.; Ferreira, P.G. Eddington's theory of gravity and its progeny. *Phys. Rev. Lett.* **2010**, *105*, 011101. [[CrossRef](#)]
36. Alishahiha, M.; Silverstein, E.; Tong, D. DBI in the sky. *Phys. Rev. D* **2004**, *70*, 123505. [[CrossRef](#)]
37. Liu, Y.X.; Yang, K.; Guo, H.; Zhong, Y. Domain Wall Brane in Eddington Inspired Born-Infeld Gravity. *Phys. Rev. D* **2012**, *85*, 124053. [[CrossRef](#)]
38. Choudhury, S.; Pal, S. DBI Galileon inflation in background SUGRA. *Nucl. Phys. B* **2013**, *874*, 85–114. [[CrossRef](#)]
39. Choudhury, S.; Pal, S. Primordial non-Gaussian features from DBI Galileon inflation. *Eur. Phys. J. C* **2015**, *75*, 241. [[CrossRef](#)]
40. Harko, T.; Lobo, F.S.N.; Mak, M.K.; Sushkov, S.V. Structure of neutron, quark and exotic stars in Eddington-inspired Born-Infeld gravity. *Phys. Rev. D* **2013**, *88*, 044032. [[CrossRef](#)]
41. Wei, S.W.; Yang, K.; Liu, Y.X. Black hole solution and strong gravitational lensing in Eddington-inspired Born-Infeld gravity. *Eur. Phys. J. C* **2015**, *75*, 253. [[CrossRef](#)]
42. Shaikh, R. Lorentzian wormholes in Eddington-inspired Born-Infeld gravity. *Phys. Rev. D* **2015**, *92*, 024015. [[CrossRef](#)]
43. Avelino, P.P. Inner Structure of Black Holes in Eddington-inspired Born-Infeld gravity: The role of mass inflation. *Phys. Rev. D* **2016**, *93*, 044067. [[CrossRef](#)]
44. Prasetyo, I.; Husin, I.; Qauli, A.I.; Ramadhan, H.S.; Sulaksono, A. Neutron stars in the braneworld within the Eddington-inspired Born-Infeld gravity. *JCAP* **2018**, *01*, 027. [[CrossRef](#)]
45. Chen, C.Y.; Bouhmadi-Lopez, M.; Chen, P. Black hole solutions in mimetic Born-Infeld gravity. *Eur. Phys. J. C* **2018**, *78*, 59. [[CrossRef](#)]
46. Shaikh, R. Wormholes with nonexotic matter in Born-Infeld gravity. *Phys. Rev. D* **2018**, *98*, 064033. [[CrossRef](#)]
47. Jana, S.; Shaikh, R.; Sarkar, S. Overcharging black holes and cosmic censorship in Born-Infeld gravity. *Phys. Rev. D* **2018**, *98*, 124039. [[CrossRef](#)]
48. Böhmer, C.G.; Fiorini, F. The regular black hole in four dimensional Born-Infeld gravity. *Class. Quant. Grav.* **2019**, *36*, 12LT01. [[CrossRef](#)]
49. Delhom, A.; Macedo, C.F.B.; Olmo, G.J.; Crispino, L.C.B. Absorption by black hole remnants in metric-affine gravity. *Phys. Rev.* **2019**, *D100*, 024016. [[CrossRef](#)]



50. Avelino, P.P.; Ferreira, R.Z. Bouncing Eddington-inspired Born-Infeld cosmologies: An alternative to Inflation? *Phys. Rev. D* **2012**, *86*, 041501. [\[CrossRef\]](#)
51. Beltrán Jiménez, J.; Heisenberg, L.; Olmo, G.J.; Rubiera-Garcia, D. Born-Infeld inspired modifications of gravity. *Phys. Rep.* **2018**, *727*, 1–129. [\[CrossRef\]](#)
52. Beltrán Jiménez, J.; Delhom, A. Ghosts in metric-affine higher order curvature gravity. *Eur. Phys. J. C* **2019**, *79*, 656. [\[CrossRef\]](#)
53. Jiménez, J.B.; Delhom, A. Instabilities in metric-affine theories of gravity with higher order curvature terms. *Eur. Phys. J.* **2020**, *C80*, 585. [\[CrossRef\]](#)
54. Delhom, A. Minimal coupling in presence of non-metricity and torsion. *Eur. Phys. J.* **2020**, *C80*, 728. [\[CrossRef\]](#)
55. Afonso, V.I.; Olmo, G.J.; Rubiera-Garcia, D. Mapping Ricci-based theories of gravity into general relativity. *Phys. Rev. D* **2018**, *97*, 021503. [\[CrossRef\]](#)
56. Jiménez, J.B.; de Andrés, D.; Delhom, A. Anisotropic deformations in a class of projectively-invariant metric-affine theories of gravity. *Class. Quant. Grav.* **2020**, *37*, 225013. [\[CrossRef\]](#)
57. Jana, S.; Chakravarty, G.K.; Mohanty, S. Constraints on Born-Infeld gravity from the speed of gravitational waves after GW170817 and GRB 170817A. *Phys. Rev. D* **2018**, *97*, 084011. [\[CrossRef\]](#)
58. Barragan, C.; Olmo, G.J. Isotropic and Anisotropic Bouncing Cosmologies in Palatini Gravity. *Phys. Rev.* **2010**, *D82*, 084015. [\[CrossRef\]](#)
59. Afonso, V.I.; Olmo, G.J.; Rubiera-Garcia, D. Scalar geons in Born-Infeld gravity. *JCAP* **2017**, *08*, 031. [\[CrossRef\]](#)
60. Solé, J.; Gómez-Valent, A.; de Cruz Pérez, J. First evidence of running cosmic vacuum: Challenging the concordance model. *Astrophys. J.* **2017**, *836*, 43. [\[CrossRef\]](#)
61. Barrow, J.D.; Basilakos, S.; Saridakis, E.N. Big Bang Nucleosynthesis constraints on Barrow entropy. *Phys. Lett.* **2021**, *B815*, 136134. [\[CrossRef\]](#)
62. Jiménez, J.B.; Delhom, A.; Olmo, G.J.; Orazi, E. Born-Infeld gravity: Constraints from light-by-light scattering and an effective field theory perspective. *Phys. Lett. B* **2021**, *820*, 136479. [\[CrossRef\]](#)
63. Latorre, A.D.I.; Olmo, G.J.; Ronco, M. Observable traces of non-metricity: New constraints on metric-affine gravity. *Phys. Lett.* **2018**, *B780*, 294–299. [\[CrossRef\]](#)
64. Delhom, A.; Miralles, V.; Peñuelas, A. Effective interactions in Ricci-Based Gravity below the non-metricity scale. *Eur. Phys. J.* **2020**, *C80*, 340. [\[CrossRef\]](#)
65. Jiménez, R.; Loeb, A. Constraining cosmological parameters based on relative galaxy ages. *Astrophys. J.* **2002**, *573*, 37–42. [\[CrossRef\]](#)
66. Moresco, M.; Verde, L.; Pozzetti, L.; Jiménez, R.; Cimatti, A. New constraints on cosmological parameters and neutrino properties using the expansion rate of the Universe to  $z = 1.75$ . *JCAP* **2012**, *1207*, 053. [\[CrossRef\]](#)
67. Moresco, M. Improved constraints on the expansion rate of the Universe up to  $z = 1.1$  from the spectroscopic evolution of cosmic chronometers. *JCAP* **2012**, *1208*, 006. [\[CrossRef\]](#)
68. Moresco, M. Raising the bar: New constraints on the Hubble parameter with cosmic chronometers at  $z = 2$ . *Mon. Not. R. Astron. Soc.* **2015**, *450*, L16–L20. [\[CrossRef\]](#)
69. Moresco, M.; Pozzetti, L.; Cimatti, A.; Jiménez, R.; Maraston, C.; Verde, L.; Thomas, D.; Citro, A.; Tojeiro, R.; Wilkinson, D. A new evidence of the epoch of cosmic re-acceleration. *JCAP* **2016**, *1605*, 014. [\[CrossRef\]](#)
70. Scolnic, D. The Complete Light-curve Sample of Spectroscopically Confirmed SNe Ia from Pan-STARRS1 and Cosmological Constraints from the Combined Pantheon Sample. *Astrophys. J.* **2018**, *859*, 101. [\[CrossRef\]](#)
71. Anagnostopoulos, F.K.; Basilakos, S.; Saridakis, E.N. Observational constraints on Barrow holographic dark energy. *Eur. Phys. J.* **2020**, *C80*, 826. [\[CrossRef\]](#)
72. Roberts, C.; Horne, K.; Hodson, A.O.; Leggat, A.D. Tests of  $\Lambda$ CDM and Conformal Gravity using GRB and Quasars as Standard Candles out to  $z_{\text{sim8}}$ . *arXiv* **2017**, arXiv:1711.10369.
73. Demianski, M.; Piedipalumbo, E.; Sawant, D.; Amati, L. Cosmology with gamma-ray bursts: I. The Hubble diagram through the calibrated  $E_{\text{rmp},i} - E_{\text{rmi},0}$  correlation. *Astron. Astrophys.* **2017**, *598*, A112. [\[CrossRef\]](#)
74. Hogg, N.B.; Martinelli, M.; Nesseris, S. Constraints on the distance duality relation with standard sirens. *arXiv* **2020**, arXiv:2007.14335.
75. Martinelli, M. Euclid: Forecast constraints on the cosmic distance duality relation with complementary external probes. *arXiv* **2020**, arXiv:2007.16153.
76. Benisty, D.; Staicova, D. Testing Low-Redshift Cosmic Acceleration with the Complete Baryon Acoustic Oscillations data collection. *arXiv* **2020**, arXiv:2009.10701.
77. Percival, W.J. Baryon Acoustic Oscillations in the Sloan Digital Sky Survey Data Release 7 Galaxy Sample. *Mon. Not. R. Astron. Soc.* **2010**, *401*, 2148–2168. [\[CrossRef\]](#)
78. Beutler, F.; Blake, C.; Colless, M.; Jones, D.H.; Staveley-Smith, L.; Campbell, L.; Parker, Q.; Saunders, W.; Watson, F. The 6dF Galaxy Survey: Baryon Acoustic Oscillations and the Local Hubble Constant. *Mon. Not. R. Astron. Soc.* **2011**, *416*, 3017–3032. [\[CrossRef\]](#)
79. Busca, N.G. Baryon Acoustic Oscillations in the Ly- $\alpha$  forest of BOSS quasars. *Astron. Astrophys.* **2013**, *552*, A96. [\[CrossRef\]](#)
80. Anderson, L. The clustering of galaxies in the SDSS-III Baryon Oscillation Spectroscopic Survey: Baryon Acoustic Oscillations in the Data Release 9 Spectroscopic Galaxy Sample. *Mon. Not. R. Astron. Soc.* **2013**, *427*, 3435–3467. [\[CrossRef\]](#)

81. Seo, H.J. Acoustic scale from the angular power spectra of SDSS-III DR8 photometric luminous galaxies. *Astrophys. J.* **2012**, *761*, 13. [\[CrossRef\]](#)
82. Ross, A.J.; Samushia, L.; Howlett, C.; Percival, W.J.; Burden, A.; Manera, M. The clustering of the SDSS DR7 main Galaxy sample '96 I. A 4 per cent distance measure at  $z = 0.15$ . *Mon. Not. R. Astron. Soc.* **2015**, *449*, 835–847. [\[CrossRef\]](#)
83. Tojeiro, R. The clustering of galaxies in the SDSS-III Baryon Oscillation Spectroscopic Survey: Galaxy clustering measurements in the low redshift sample of Data Release 11. *Mon. Not. R. Astron. Soc.* **2014**, *440*, 2222–2237. [\[CrossRef\]](#)
84. Bautista, J.E. The SDSS-IV extended Baryon Oscillation Spectroscopic Survey: Baryon Acoustic Oscillations at redshift of 0.72 with the DR14 Luminous Red Galaxy Sample. *Astrophys. J.* **2018**, *863*, 110. [\[CrossRef\]](#)
85. de Carvalho, E.; Bernui, A.; Carvalho, G.C.; Novaes, C.P.; Xavier, H.S. Angular Baryon Acoustic Oscillation measure at  $z = 2.225$  from the SDSS quasar survey. *JCAP* **2018**, *1804*, 064. [\[CrossRef\]](#)
86. Ata, M. The clustering of the SDSS-IV extended Baryon Oscillation Spectroscopic Survey DR14 quasar sample: First measurement of baryon acoustic oscillations between redshift 0.8 and 2.2. *Mon. Not. R. Astron. Soc.* **2018**, *473*, 4773–4794. [\[CrossRef\]](#)
87. Abbott, T.M.C. Dark Energy Survey Year 1 Results: Measurement of the Baryon Acoustic Oscillation scale in the distribution of galaxies to redshift 1. *Mon. Not. R. Astron. Soc.* **2019**, *483*, 4866–4883. [\[CrossRef\]](#)
88. Molavi, Z.; Khodam-Mohammadi, A. Observational tests of Gauss-Bonnet like dark energy model. *Eur. Phys. J. Plus* **2019**, *134*, 254. [\[CrossRef\]](#)
89. Riess, A.G.; Casertano, S.; Yuan, W.; Bowers, J.B.; Macri, L.; Zinn, J.C.; Scolnic, D. Cosmic Distances Calibrated to 1Parallaxes and Hubble Space Telescope Photometry of 75 Milky Way Cepheids Confirm Tension with  $\Lambda$ CDM. *Astrophys. J. Lett.* **2021**, *908*, L6. [\[CrossRef\]](#)
90. Foreman-Mackey, D.; Hogg, D.W.; Lang, D.; Goodman, J. emcee: The MCMC Hammer. *Publ. Astron. Soc. Pac.* **2013**, *125*, 306–312. [\[CrossRef\]](#)
91. Handley, W.J.; Hobson, M.P.; Lasenby, A.N. PolyChord: Nested sampling for cosmology. *Mon. Not. R. Astron. Soc.* **2015**, *450*, L61–L65. [\[CrossRef\]](#)
92. Lewis, A. GetDist: A Python package for analysing Monte Carlo samples. *arXiv* **2019**, arXiv:1910.13970.
93. Beltran Jimenez, J.; Heisenberg, L.; Olmo, G.J.; Rubiera-Garcia, D. On gravitational waves in Born-Infeld inspired non-singular cosmologies. *JCAP* **2017**, *10*, 29. [\[CrossRef\]](#)
94. Escamilla-Rivera, C.; Banados, M.; Ferreira, P.G. A tensor instability in the Eddington inspired Born-Infeld Theory of Gravity. *Phys. Rev. D* **2012**, *85*, 087302. [\[CrossRef\]](#)